I&EC research
Industrial & Engineering Chemistry Research
pubs.acs.org/IECR
Article

Model Predictive Control of Jacket Tubular Reactors with a Reversible Exothermic Reaction

Lu Zhang, Junyao Xie, Charles Robert Koch, and Stevan Dubljevic*

Cite This: *Ind. Eng. Chem. Res.* 2020, 59, 18921−18936
Read Online
ACCESS | Metrics & More | Article Recommendations | Supporting Information

ABSTRACT: This article addresses the model predictive controller design for a jacket tubular reactor with a simple reversible exothermic reaction ($A \rightleftharpoons B$). Using energy and mass balance laws, four nonlinear hyperbolic partial differential equations are derived to model the tubular reactor dynamics in terms of two concentrations, the reactor temperature, and the spatially varying jacket temperature. The nonlinear continuous-time model is linearized and discretized in time by the use of the Cayley−Tustin transform without spatial discretization or model reduction. Along these lines, a state-feedback model predictive controller is formulated to realize model stabilization with respect to input and output constraints. To account for the state estimation, a Luenberger observer-based model predictive control (MPC) frame is further developed, and observer gains are obtained as solutions of an operator Riccati equation. Finally, two numerical examples are provided to demonstrate the feasibility and applicability of the proposed MPC designs.

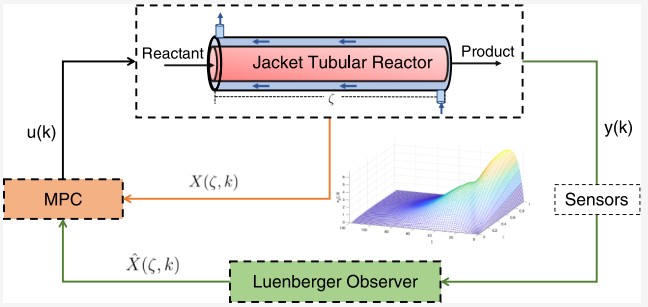

INTRODUCTION

Tubular reactors play a significant role in chemical engineering practice. Models of various types of tubular reactors are usually described by nonlinear partial differential equations (PDEs) derived from conservation laws, which originated from mass and energy balances and which belong to the class of distributed parameter systems (DPSs).[1] The salient feature of these models is temporal- and spatial-state dependence that capture the kinetic properties within the reactors and can be connected with the phase change, generation, and/or consumption of chemical species.[2]

Because of the numerous industrial applications of tubular reactors, the corresponding issues of modeling and controlling are of great importance for the safety and economic operations,[3−6] and hence have been explored in many studies over the years. For instance, a series of contributions were focused on the first-order exothermic irreversible reaction $A \rightarrow bB$ within the uniform jacket tubular reactors.[7−9] An ideal plug-flow tubular reactor having a simple exothermic consecutive reaction $A \rightarrow B \rightarrow C$ with cocurrent cooling[10] and of $A + B \rightarrow C$ with advection and axial diffusion were further investigated.[11] In addition, the reversible reactions $aA \rightleftharpoons rR$ were widely studied, especially in chemical and biological processes, such as polymerization and isomerization, enzyme kinetics, and racemization of molecules with mirror-image structures.[12−14] Based on the mathematical models of various reaction systems, significant research efforts have been made toward control designs.[15,16] In particular, a globally stabilizing boundary feedback control law was developed to stabilize the unstable steady states of temperature and concentration on the inlet side of the tubular reactor.[17] Furthermore, the backstepping-based infinite-dimensional observers were proposed for a class of linear parabolic PDEs.[18] Along the same lines, the dynamic analysis and linear quadratic optimal control were extensively developed for a class of tubular reactors.[7,19,20] However, when it comes to the controller design for reversible reaction systems, there is limited attention in the research literature.[12,21−23] The inevitable difficulty comes from the infinite-dimensional nature of heterodirectional hyperbolic systems, which is a limiting factor when controller designs and monitoring realizations are considered. Motivated by these observations, the objective of our article is the simple reversible reaction, which is described by the nonlinear coupled 4 × 4 hyperbolic PDEs.

Considering the typical requirements for the operation of tubular reactors in practice, such as the temperature and concentration of reactants not exceeding certain ranges, as well as the physical limits of actuators or sensors, model predictive control (MPC) as a popular and widely deployed methodology in the process industry is capable of handling such requirements. The main idea of MPC can be dated back to the 1960s and its application originated in the chemical industry in the

Received: May 18, 2020
Revised: September 15, 2020
Accepted: September 30, 2020
Published: October 13, 2020

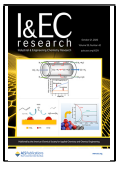

https://dx.doi.org/10.1021/acs.iecr.0c02500
Ind. Eng. Chem. Res. 2020, 59, 18921−18936

1970s.[24] Basically, a model of interest is implemented as an optimization problem, which is then solved to determine the best set of inputs for decisions. The optimization problem needs to be reformulated iteratively as time increases, and only the first input is implemented every time. Over the past two decades, MPC has been extensively used in linear and nonlinear finite-dimensional systems.[25,26] MPC theory is now a mature body of knowledge encompassing the stability and robustness of linear and nonlinear models, which has a significant impact on industrial process control and has been extended to the control of infinite-dimensional systems, especially tubular reactor systems.[27,28] More specifically, a nonlinear MPC for a tubular reactor was developed by combining data-driven and model-reduction approaches, where the proper orthogonal decomposition (POD) and finite-element Galerkin projection methods were applied to approximate the PDE system.[29] Similar methods (POD and Galerkin projection) were utilized to derive the low-order linear model that captures the dominant dynamics of the PDEs, which were subsequently used for the MPC design of distributed reactor models with axial and radial diffusion.[30] An economic MPC framework was proposed for a tubular reactor and the reduced-order model was constructed based on the basis of historical data-based empirical eigenfunctions and Galerkin's method.[31] However, these approaches are only applicable for the Riesz spectral systems (parabolic and higher order dissipative PDEs) and not suitable for nonspectral systems, such as the hyperbolic PDEs. There are other extensions in this area, for instance, a nonlinear MPC scheme for continuous emulsion co-polymerization in a tubular reactor was presented,[32] where the PDEs were converted to a system of ODEs using the method of lines. A general nonlinear MPC framework for low-density polyethylene tubular reactors was developed,[33] where the cascade PDEs−ODEs system was discretized in space and time for implementation using the implicit Euler and finite-element scheme. In addition, there are some other works on linear model predictive controller designs of transport reaction systems based on online model reduction[34,35] and the structure-preserving discretization framework.[9,36,37]

Most of the aforementioned works depend on spatial approximation (discretization) in the controller design stage. However, the main drawback of these approaches lies in the fact that the spatial discretization might induce numerical instability, and/or the fundamental control theoretical properties (controllability, observability, and stability) might be lost and/or altered significantly.[1,38] On the other hand, the obtained discrete model can only provide approximate states at the spatial discretization points instead of the spatial states between discretized points. In general, these approaches belong to early lumping, as spatial discretization needs to be preformed in the design stage. In contrast, late lumping takes full advantage of the available distributed parameter control theory and utilizes the infinite-dimensional setting for the controller design, and only performs lumping along some spatial approximation for the purpose of implementation.

In a late lumping manner, the Cayley−Tustin time-discretization framework was proposed by Havu and Malinen,[39,40] which was demonstrated to be a symmetric and symplectic integration scheme that ensures energy and structure preservation. Another novel energy-preserving approach was introduced by Lefevre and coworkers.[41−43] Their method of spatial discretization for infinite-dimensional port-Hamiltonian systems can preserve the model structure during the model reduction and consist of splitting the initial structured infinite-dimensional model into N finite-dimensional submodels with the same energetic behavior.[41] Compared with the Cayley−Tustin time-discretization method, the main similarity is that both approaches guarantee structure-preserving numerical integration. The main difference is that the Cayley−Tustin time-discretization method does not alter the system theoretical properties (such as stability, controllability, and observability) which play a significant role in the controller design.[42,44] The discretization framework proposed by Lefevre and coworkers can preserve the stability, while the preservation of controllability and observability during discretization is not investigated.[41−43]

Motivated by the aforementioned considerations, we extend the finite-dimensional MPC setting to the jacket tubular reactor with a simple reversible reaction modeled by the 4×4 hyperbolic PDEs and, in particular, the Cayley−Tustin method is utilized for time discretization of the continuous hyperbolic PDE model, and in the linear MPC controller design in a late lumping manner, which achieves a satisfactory performance with respect to the input and output constraints and accounts for constrained stabilization of the disturbed system.

The five contributions of this work are summarized next: (1) a PDE model is established for a jacked tubular reactor with consideration of a simple reversible reaction ($A \rightleftharpoons B$), which is a common practice in chemical engineering but has not been fully investigated in the literature as it accounts for the heterodirectional hyperbolic systems. (2) A spatially varying jacket temperature is considered instead of the uniformly distributed jacket temperature along with the concentration of reactants and products, and the temperature of the reactor reflects the spatiotemporal dynamics of the reactor system. (3) Cayley−Tustin time discretization is utilized to preserve the system properties (such as stability, controllability, and observability). (4) A full-state feedback MPC controller is designed and implemented to address the physical constraints in actuators and sensors. (5) Considering the common scenario of unavailability of full-state information and the existence of disturbance, an observer-based MPC is designed using the state estimated by the Luenberger observer and finding the observer gain by solving an operator Riccati equation.

The organization of this paper is described next. In the Problem Formulation section, the infinite-dimensional-state space model is introduced. Furthermore, the linearized model and Cayley−Tustin time discretization for the tubular reactor are provided. In the MPC Formulation section, the model predictive controllers are designed including state-feedback MPC and observer-based MPC. Finally, in the Simulation Study section, the performances of the presented state-feedback MPC and observer-based MPC are demonstrated by two numerical examples, where the influence of constraints, penalty weights, and disturbances on the MPC performance is further analyzed.

Problem Formulation. In this section, we introduce the problem formulation. First, the mathematical model of the jacketed tubular reactor is presented with a simple reversible reaction taking place. Second, the model linearization around the equilibrium point is proposed to construct a linearized model. Finally, the discrete-time infinite-dimensional model is obtained utilizing the Cayley−Tustin transform framework.

https://dx.doi.org/10.1021/acs.iecr.0c02500
Ind. Eng. Chem. Res. 2020, 59, 18921−18936

Model Description. Figure 1 shows a schematic of a tubular reactor. This tubular reactor is a nonisothermal reactor, where an elementary exothermic first-order reversible reaction takes place ($A \rightleftharpoons B$).

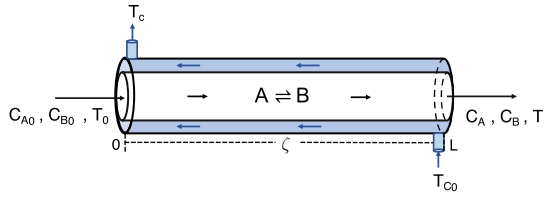

Figure 1. Jacket tubular reactor representation.

The mathematical model for the considered tubular reactor is based on the following assumptions. (1) Uniform radial velocity and distribution. (2) Uniform radial temperature and concentration distribution. (3) Constant density and volume of the liquid within the reactor. The heat capacities of the reactant, diffusion, and dispersion are neglected.

Under these simplifying assumptions, the dynamics of the process are typically described by the following four nonlinear PDEs which are derived from energy and mass balance principles.[27,45,46] In particular, one considers the spatially varying jacket temperature that can be described by another hyperbolic PDE.

$$\begin{aligned}
\frac{\partial C_A(\zeta, t)}{\partial t} &= -v\frac{\partial C_A(\zeta, t)}{\partial \zeta} - k_1 e^{-E_1/T(\zeta,t)R} C_A(\zeta, t) \\
&\quad + k_2 e^{-E_2/T(\zeta,t)R} C_B(\zeta, t) \\
\frac{\partial C_B(\zeta, t)}{\partial t} &= -v\frac{\partial C_B(\zeta, t)}{\partial \zeta} + k_1 e^{-E_1/T(\zeta,t)R} C_A(\zeta, t) \\
&\quad - k_2 e^{-E_2/T(\zeta,t)R} C_B(\zeta, t) \\
\frac{\partial T(\zeta, t)}{\partial t} &= -v\frac{\partial T(\zeta, t)}{\partial \zeta} + \frac{-\Delta H}{\rho C_p} k_1 e^{-E_1/T(\zeta,t)R} C_A(\zeta, t) \\
&\quad - \frac{-\Delta H}{\rho C_p} k_2 e^{-E_2/T(\zeta,t)R} C_B(\zeta, t) \\
&\quad + \frac{U}{\rho C_p V}(T_c(\zeta, t) - T(\zeta, t)) \\
\frac{\partial T_c(\zeta, t)}{\partial t} &= v_c\frac{\partial T_c(\zeta, t)}{\partial \zeta} - \frac{U}{\rho C_p V}(T_c(\zeta, t) - T(\zeta, t)) \\
&\quad + b(\zeta)\bar{u}(t)
\end{aligned} \tag{1}$$

In these equations, C_A, C_B denote the concentrations of the reactant and the product, respectively. The temperature inside of the reactor is T and T_c is the temperature of the cooling medium flowing around the wall of the tubular reactor. The symbols v, v_c, E_1, E_2, k_1, k_2, R, ΔH, ρC_p, U, and V denote the superficial fluid velocity, the velocity of the cooling fluid, the activation energy of the reactant and the product, the kinetic constant of A and B, the ideal gas constant, the enthalpy, the constant heat capacity, the product of the density and the heat capacity of the fluid in the reactor, the heat-transfer coefficient, and the volume of the reactor, respectively.[47] Parameters of the reactor considered are shown in Table 1.

In addition, ζ ($\zeta \in [0, L]$), and t ($t \in [0, \infty)$) denote the spatial variable and the temporal variable, respectively. The boundary actuation is $\bar{u}(t)$, and it is characterized by $b(\zeta)$, which is given as $b(\zeta) = \frac{1}{2\bar{\zeta}_L} 1_{[\zeta_L - \bar{\zeta}_L, \zeta_L + \bar{\zeta}_L]}(\zeta)$. In summary, the controlled variables are the concentrations C_A, C_B and the temperature T of the reactor, and the corresponding manipulated variable is the inlet flow temperature of the jacket. The mathematical model in eq 1 represents a nonlinear relation between controlled variables and manipulated variables.

Table 1. Notation and Values of Parameters

process parameters	notations	numerical values
fluid velocity in the reactor	v	0.025 m/s
fluid velocity in the jacket	v_c	0.1 m/s
length of the reactor	L	1 m
activation energy of the reactant	E_1	46.15 kJ/mol
activation energy of the product	E_2	209.29 kJ/mol
heat-transfer parameter	$U/\rho C_p V$	0.2 s^{-1}
idea gas constant	R	8.314 J/(mol·K)
stoichiometric coefficient	$-\Delta H/\rho C_p$	−4250 K·L/mol

Correspondingly, the following boundary conditions are considered

$$\begin{aligned}
&C_A(0, t) = C_{A_0}, \; C_B(0, t) = 0, \; T(0, t) = T_0, \; T_c(L, t) \\
&\quad = T_{C_0}
\end{aligned} \tag{2}$$

with the given initial conditions

$$\begin{aligned}
&C_A(\zeta, 0) = C_A(\zeta), \; C_B(\zeta, 0) = 0, \; T(\zeta, 0) = T(\zeta), \\
&\quad T_c(\zeta, 0) = T_c(\zeta)
\end{aligned} \tag{3}$$

The output is taken in the following form

$$y(t) = C\begin{bmatrix} C_A(\zeta, t) \\ C_B(\zeta, t) \\ T(\zeta, t) \\ T_c(\zeta, t) \end{bmatrix} \tag{4}$$

where $C(\cdot) = \mathrm{diag}\left\{ \int_0^L (\cdot)\delta(\zeta - L)\mathrm{d}\zeta, \int_0^L (\cdot)\delta(\zeta - L)\mathrm{d}\zeta, \int_0^L (\cdot)\delta(\zeta - L)\mathrm{d}\zeta, \int_0^L (\cdot)\delta(\zeta)\mathrm{d}\zeta \right\}$ and $\delta(\zeta)$ is the Dirac function which can capture the spatial measurement points of interest.

System Linearization. The mathematical model described above is composed of a set of PDEs that accurately describe the dynamics of the tubular reactor from spatial and temporal dimensional. It is, however, a fully coupled and nonlinear PDE model that is difficult to solve directly and analyze further. Linearizing this system around some steady states of interest is one way to proceed.[9]

First, the steady-state model of eq 1 can be simply obtained as the time $t \to \infty$, which means that all derivatives with respect to time are equal to zero.

https://dx.doi.org/10.1021/acs.iecr.0c02500
Ind. Eng. Chem. Res. 2020, 59, 18921−18936

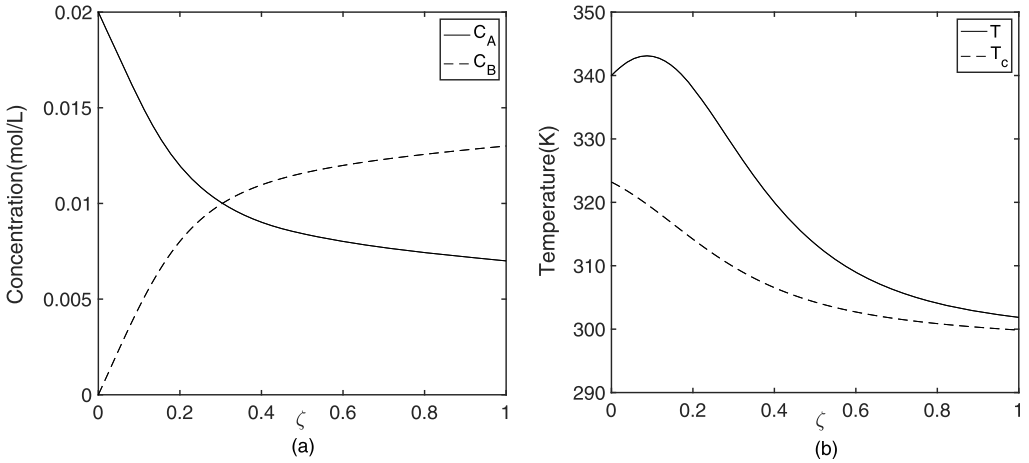

Figure 2. Steady-state profiles of the tubular reactor.

$$
\begin{aligned}
&-v\frac{\partial C_{A_{ss}}}{\partial \zeta} - k_1 e^{-E_1/T_{ss}R} C_{A_{ss}} + k_2 e^{-E_2/T_{ss}R} C_{B_{ss}} = 0\\
&-v\frac{\partial C_{B_{ss}}}{\partial \zeta} + k_1 e^{-E_1/T_{ss}R} C_{A_{ss}} - k_2 e^{-E_2/T_{ss}R} C_{B_{ss}} = 0\\
&-v\frac{\partial T_{ss}}{\partial \zeta} + \frac{-\Delta H}{\rho C_p} k_1 e^{-E_1/T_{ss}R} C_{A_{ss}} - \frac{-\Delta H}{\rho C_p} k_2 e^{-E_2/T_{ss}R} C_{B_{ss}}\\
&\quad + \frac{U}{\rho C_p V}(T_{c_{ss}} - T_{ss}) = 0\\
&v_c\frac{\partial T_{c_{ss}}}{\partial \zeta} - \frac{U}{\rho C_p V}(T_{c_{ss}} - T_{ss}) = 0
\end{aligned}
\tag{5}
$$

The steady states can be solved numerically by the finite difference method. More specifically, the derivatives with respect to the axial variable can be replaced by the first-order backward and the first-order forward differences. As a result, the corresponding steady-state profiles are illustrated in Figure 2.

By applying the state transformation and linearization, the original nonlinear PDEs in eq 1 can be linearized around the steady states.

$$
X = \begin{bmatrix} x_1(\zeta,\ t)\\ x_2(\zeta,\ t)\\ x_3(\zeta,\ t)\\ x_4(\zeta,\ t)\end{bmatrix} = \begin{bmatrix} C_A(\zeta,\ t) - C_{A_{ss}}(\zeta,\ t)\\ C_B(\zeta,\ t) - C_{B_{ss}}(\zeta,\ t)\\ T(\zeta,\ t) - T_{ss}(\zeta,\ t)\\ T_c(\zeta,\ t) - T_{c_{ss}}(\zeta,\ t)\end{bmatrix} \tag{6}
$$

Moreover, the steady states $C_{A_{ss}}$, $C_{B_{ss}}$, T_{ss}, and $T_{c_{ss}}$ need to satisfy their corresponding boundary conditions indicated in eq 2. Therefore, the linearized infinite-dimensional model is obtained in the following form

$$
\frac{\partial X(\zeta,\ t)}{\partial t} = V\frac{\partial X(\zeta,\ t)}{\partial \zeta} + A(\zeta)X(\zeta,\ t) + B(\zeta)u(t) \tag{7}
$$

where $u(t)$ is the corresponding input action of the linearized system and the following notations are used in this equation.

$$
\begin{aligned}
&V = \mathrm{diag}\{-v,\ -v,\ -v,\ v_c\},\\
&A(\zeta) = \begin{bmatrix} -N_1 & N_2 & -G_1 & 0\\ N_1 & -N_2 & G_1 & 0\\ \beta N_1 & -\beta N_2 & G_2 & \alpha\\ 0 & 0 & \alpha & -\alpha\end{bmatrix},\\
&B(\zeta) = [0;\ 0;\ 0;\ b(\zeta)], \quad \alpha = \frac{U}{\rho C_p V},\\
&\beta = \frac{-\Delta H}{\rho C_p}, \quad \mu_1 = \frac{E_1}{R}, \quad \mu_2 = \frac{E_2}{R},\\
&N_1 = k_1 e^{-\mu_1/T_{ss}}, \quad N_2 = k_2 e^{-\mu_2/T_{ss}},\\
&G_1 = N_1\mu_1\frac{C_{A_{ss}}}{T_{ss}^2} - N_2\mu_2\frac{C_{B_{ss}}}{T_{ss}^2},\\
&G_2 = \beta N_1\mu_1\frac{C_{A_{ss}}}{T_{ss}^2} - \beta N_2\mu_2\frac{C_{B_{ss}}}{T_{ss}^2} - \alpha
\end{aligned}
\tag{8}
$$

The linearized system has the corresponding boundary conditions of

$$
x_1(0,\ t) = 0,\ x_2(0,\ t) = 0,\ x_3(0,\ t) = 0,\ x_4(L,\ t) = 0 \tag{9}
$$

and the initial conditions

$$
\begin{aligned}
&x_1(\zeta,\ 0) = C_A(\zeta) - C_{A_{ss}}(\zeta),\\
&x_2(\zeta,\ 0) = C_B(\zeta) - C_{B_{ss}}(\zeta)\\
&x_3(\zeta,\ 0) = T(\zeta) - T_{ss}(\zeta),\\
&x_4(\zeta, 0) = T_c(\zeta) - T_{c_{ss}}(\zeta)
\end{aligned}
\tag{10}
$$

The linearized jacket tubular reactor model is now complete and the standard infinite-dimensional continuous-time state-space model can be formulated as

$$
\begin{aligned}
\dot{X}(\zeta, t) &= \mathcal{A}X(\zeta,\ t) + \mathcal{B}u(t)\\
Y(t) &= CX(\zeta,\ t)
\end{aligned}
\tag{11}
$$

subject to the boundary conditions eq 9 and the initial conditions eq 10. The state $X(\zeta,\ t)\in\mathcal{X}$, with

https://dx.doi.org/10.1021/acs.iecr.0c02500
Ind. Eng. Chem. Res. 2020, 59, 18921−18936

$\mathcal{X} = L^2((0,\ L), \mathbb{R}^4)$ being defined as a real separable Hilbert space with the inner product $\langle\cdot,\cdot\rangle$. The input

$$u(t) \in {L_{\text{loc}}}^2([0,\ \infty),\ \mathcal{U})$$

and output

$$y(t) \in {L_{\text{loc}}}^2([0,\ \infty),\ \mathcal{Y})$$

where $\mathcal{U}$ and $\mathcal{Y}$ are real separable Hilbert spaces.

In this form, one can define the operator $\mathcal{A}(\cdot) = V\frac{\partial(\cdot)}{\partial\zeta} + A(\zeta)(\cdot)$ on its domain. $\mathcal{A}$ is the infinitesimal generator of a C_0-semigroup on $\mathcal{X}$. Also, the input operator $\mathcal{B}$ is defined as a bounded operator $\mathcal{B} = [0;\ 0;\ 0;\ b(\zeta)]$. The operator $\mathcal{B}$ can approximate "point actuation" using a small interval shape function.[48] To construct the model predictive controller in the next section, the adjoint operator of $\mathcal{A}$ needs to be predetermined. For this system, the adjoint operator $\mathcal{A}^*$ is easily found using the inner product formula,

$$\langle\mathcal{A}\varphi,\ \phi\rangle = \langle\varphi,\ \mathcal{A}^*\phi\rangle,$$

and is given by

$$\mathcal{A}^*(\cdot) = -V\frac{\partial(\cdot)}{\partial\zeta} + A^*(\zeta)(\cdot) \tag{12}$$

with its domain defined as $\mathcal{D}(\mathcal{A}^*) = \{\phi = [\phi_1;\ \phi_2;\ \phi_3;\ \phi_4] \mid \phi_i(\zeta) \in L_2(0,\ 1),\ \phi_i(\zeta)$ is absolutely continuous, $\mathrm{d}\phi_i/\mathrm{d}\zeta \in L_2(0,\ 1)$, with $i = 1, 2, 3, 4$, and $\phi_1(1) = 0,\ \phi_2(1) = 0,\ \phi_3(1) = 0,\ \phi_4(0) = 0\}$.

The output is obtained as

$$Y(t) = C\begin{bmatrix} x_1(\zeta,\ t) + C_{A_{ss}}(\zeta) \\ x_2(\zeta,\ t) + C_{B_{ss}}(\zeta) \\ x_3(\zeta,\ t) + T_{ss}(\zeta) \\ x_4(\zeta,\ \zeta t) + T_{c_{ss}}(\zeta) \end{bmatrix} = C\begin{bmatrix} x_1 \\ x_2 \\ x_3 \\ x_4 \end{bmatrix} + \begin{bmatrix} C_{A_{ss}}(L) \\ C_{B_{ss}}(L) \\ T_{ss}(L) \\ T_{c_{ss}}(0) \end{bmatrix} \tag{13}$$

In an analogous manner, by

$$\langle C\varphi,\ \phi\rangle = \langle\varphi,\ C^*\phi\rangle,$$

the C^* operator is determined as

$$C^*(\cdot) = \mathrm{diag}\left\{\delta(\zeta - L)\int_0^L (\cdot)\mathrm{d}\eta,\ \delta(\zeta - L)\int_0^L (\cdot)\mathrm{d}\eta,\ \delta(\zeta)\int_0^L (\cdot)\mathrm{d}\eta\right\} \tag{14}$$

Model Discretization. Based on the linearized infinite-dimensional system, we introduce the Cayley−Tustin discretization framework to transform the continuous-time system to the discrete-time one. Let us consider the above linear system in eq 11 and the given time discretization $h > 0$, and the Cayley−Tustin discretization is given by

$$\frac{X(jh) - X((j-1)h)}{h} \approx \mathcal{A}\frac{X(jh) + X((j-1)h)}{2} + \mathcal{B}u(jh),\ X(0) = X_0$$
$$Y(jh) \approx \mathcal{A}\frac{X(jh) + X((j-1)h)}{2} \tag{15}$$

for $j \geq 1$, where we omit the spatial dependence of x for brevity. Then, let $\frac{u_j^{(h)}}{\sqrt{h}}$ be an approximation of $u(jh)$ by the mean value within a given sampling time, $\frac{u_j^{(h)}}{\sqrt{h}} = \frac{1}{h}\int_{(j-1)h}^{jh} u(t)\mathrm{d}t$. It has been shown in ref 39 that $\frac{u_j^{(h)}}{\sqrt{h}}$ converges to $u(jh)$ as $h \to 0$ in several different ways, similar to $Y(jh)$. Furthermore, rewriting eq 15 gives the discrete time dynamics eq 16. It is frequently called Tustin discretization in the engineering literature, which is discovered in 1940s by Tustin and is referred to as Tustin transform in digital and sample-data control literature.[38]

$$\frac{X_j^{(h)} - X_{j-1}^{(h)}}{h} \approx \mathcal{A}\frac{X_j^{(h)} + X_{j-1}^{(h)}}{2} + \mathcal{B}\frac{u_j^{(h)}}{\sqrt{h}},\ X_0^{(h)} = X_0$$
$$\frac{Y_j^{(h)}}{\sqrt{h}} \approx C\frac{X_j^{(h)} + X_{j-1}^{(h)}}{2} \tag{16}$$

Through some basic computations, the following infinite-dimensional discrete-time state-space model is obtained

$$X_j^{(h)} = \mathcal{A}_{\mathrm{d}}X_{j-1}^{(h)} + \mathcal{B}_{\mathrm{d}}u_j^{(h)}$$
$$Y_j^{(h)} = C_{\mathrm{d}}X_{j-1}^{(h)} + \mathcal{D}_{\mathrm{d}}u_j^{(h)} \tag{17}$$

where $\mathcal{A}_{\mathrm{d}}$, $\mathcal{B}_{\mathrm{d}}$, C_{d}, and $\mathcal{D}_{\mathrm{d}}$ are the discrete-time spatial operators and are given by

$$\begin{pmatrix} \mathcal{A}_{\mathrm{d}} & \mathcal{B}_{\mathrm{d}} \\ C_{\mathrm{d}} & \mathcal{D}_{\mathrm{d}} \end{pmatrix} = \begin{pmatrix} [\delta - \mathcal{A}]^{-1}[\delta - \mathcal{A}] & \sqrt{2\delta}[\delta - \mathcal{A}]^{-1}\mathcal{B} \\ \sqrt{2\delta}C[\delta - \mathcal{A}]^{-1} & C[\delta - \mathcal{A}]^{-1}\mathcal{B} \end{pmatrix} \tag{18}$$

where $\delta = 2/h$ and the resolvent is $\mathcal{R}(\delta,\ \mathcal{A}) = (\delta I - \mathcal{A})^{-1}$. Clearly, one must satisfy $\delta \in \rho(\mathcal{A})$ so that the resolvent operator is well-defined. In particular, $C(\delta - \mathcal{A})^{-1}\mathcal{B}$ denotes the transfer function of the linearized continuous model. The unbounded operators $\mathcal{A}$ of the continuous-time system are mapped into bounded operators $\mathcal{A}_{\mathrm{d}}$ in the discrete-time counterpart through the Cayley transform. In addition, it has been demonstrated that the controllability and the stability are invariant under this transformation.[9] The continuous state evolutional operator $\mathcal{A}$ is discretized in time and $\mathcal{A}_{\mathrm{d}}$ can be described by the resolvent operator with

$$\mathcal{A}_{\mathrm{d}}(\cdot) = [\delta I - \mathcal{A}]^{-1}[\delta I + \mathcal{A}](\cdot) = -I(\cdot) + 2\delta[\delta I - \mathcal{A}]^{-1}(\cdot) = -I(\cdot) + 2\delta\mathcal{R}(\delta,\ \mathcal{A})(\cdot)$$

where I is an identity operator.

Resolvent Operator. In order to obtain the above discrete-time spatial operators which are generated by the Cayley−Tustin discretization, the resolvent operator needs to be determined. In general, there is a link between the resolvent operator and the analytical solution in the Laplace-domain for the continuous-time model, such as $\mathcal{R}(s,\ \mathcal{A})(\cdot) = [sI - \mathcal{A}]^{-1}(\cdot)$, which means one can obtain the resolvent operator by applying the Laplace transform. To better understand the resolvent operator, let us consider the following model

https://dx.doi.org/10.1021/acs.iecr.0c02500
Ind. Eng. Chem. Res. 2020, 59, 18921−18936

$$\dot{z}(\zeta,\ t) = \mathcal{A}z(\zeta,\ t),\ z(\zeta,\ 0) = z_0(\zeta) \tag{19}$$

where $\mathcal{A}$ is defined as a spatial derivative operator. Through applying the Laplace transform, one attains the associated resolvent operator $\mathcal{R}(s,\ \mathcal{A})$ as follows

$$z(\zeta,\ s) = [sI - \mathcal{A}]^{-1}z_0(\zeta) = \mathcal{R}(s,\ \mathcal{A})z_0(\zeta) \tag{20}$$

This illustrates that the resolvent operator is mapping the initial condition $z_0(\zeta)$ to the solution $z(\zeta, s)$ in the Laplace-domain.

Following this line, for the linearized hyperbolic PDEs in eq 7, the Laplace transform is applied giving

$$\frac{\partial X(\zeta,\ s)}{\partial \zeta} = FX(\zeta,\ s) - V^{-1}X(\zeta,\ 0) \tag{21}$$

where

$$F = V^{-1}[(SI - A(\zeta)] = \begin{bmatrix} -\frac{s+N_1}{\nu} & \frac{N_2}{\nu} & -\frac{G_1}{\nu} & 0 \\ \frac{N_1}{\nu} & -\frac{s+N_2}{\nu} & \frac{G_1}{\nu} & 0 \\ \frac{\beta N_1}{\nu} & -\frac{\beta N_2}{\nu} & \frac{s+G_2}{\nu} & \frac{\alpha}{\nu} \\ 0 & 0 & -\frac{\alpha}{\nu_c} & \frac{s+\alpha}{\nu_c} \end{bmatrix}$$

and V is defined in eq 8. Because of the diagonal form of V, it is clear that V is invertible, which means that the well-posedness is guaranteed. Based on the semigroup operator theory,[48] a frequency-domain solution is generated under the zero-input condition as follows

$$\begin{bmatrix} x_1(\zeta,\ s) \\ x_2(\zeta,\ s) \\ x_3(\zeta,\ s) \\ x_4(\zeta,\ s) \end{bmatrix} = e^{F\zeta}\begin{bmatrix} x_1(0,\ s) \\ x_2(0,\ s) \\ x_3(0,\ s) \\ x_4(0,\ s) \end{bmatrix} - \int_0^\zeta e^{F(\zeta-\eta)}V^{-1}\begin{bmatrix} x_1(\eta,\ 0) \\ x_2(\eta,\ 0) \\ x_3(\eta,\ 0) \\ x_4(\eta,\ 0) \end{bmatrix} d\eta \tag{22}$$

For notational simplicity, $e^{F\zeta}$ can be denoted as $e^{F\zeta} = [F_{ij}(\zeta, s)]_{4\times4}$ with $i, j = 1, 2, 3, 4$. The frequency-domain solution of the DPS is

$$\begin{bmatrix} x_1(\zeta,s) \\ x_2(\zeta,s) \\ x_3(\zeta,s) \\ x_4(\zeta,s) \end{bmatrix} = \begin{bmatrix} F_{11}(\zeta,s) & F_{12}(\zeta,s) & F_{13}(\zeta,s) & F_{14}(\zeta,s) \\ F_{21}(\zeta,s) & F_{22}(\zeta,s) & F_{23}(\zeta,s) & F_{24}(\zeta,s) \\ F_{31}(\zeta,s) & F_{32}(\zeta,s) & F_{33}(\zeta,s) & F_{34}(\zeta,s) \\ F_{41}(\zeta,s) & F_{42}(\zeta,s) & F_{43}(\zeta,s) & F_{44}(\zeta,s) \end{bmatrix}\begin{bmatrix} x_1(0,s) \\ x_2(0,s) \\ x_3(0,s) \\ x_4(0,s) \end{bmatrix} + \int_0^\zeta \begin{bmatrix} F_{11}(\zeta-\eta,s) & F_{12}(\zeta-\eta,s) & F_{13}(\zeta-\eta,s) & F_{14}(\zeta-\eta,s) \\ F_{21}(\zeta-\eta,s) & F_{22}(\zeta-\eta,s) & F_{23}(\zeta-\eta,s) & F_{24}(\zeta-\eta,s) \\ F_{31}(\zeta-\eta,s) & F_{32}(\zeta-\eta,s) & F_{33}(\zeta-\eta,s) & F_{34}(\zeta-\eta,s) \\ F_{41}(\zeta-\eta,s) & F_{42}(\zeta-\eta,s) & F_{43}(\zeta-\eta,s) & F_{44}(\zeta-\eta,s) \end{bmatrix}\begin{bmatrix} \frac{1}{\nu} & 0 & 0 & 0 \\ 0 & \frac{1}{\nu} & 0 & 0 \\ 0 & 0 & \frac{1}{\nu} & 0 \\ 0 & 0 & 0 & -\frac{1}{\nu_c} \end{bmatrix}\begin{bmatrix} x_1(\eta,0) \\ x_2(\eta,0) \\ x_3(\eta,0) \\ x_4(\eta,0) \end{bmatrix} d\eta \tag{23}$$

Considering that the corresponding boundary conditions (eq 9) are bidirectional, one needs to convert them to one side in order to determine the resolvent operator as follows

(1) At $\zeta = 0$, one can substitute $x_1(0, s) = 0$, $x_2(0, s) = 0$, and $x_3(0, s) = 0$ in eq 23, which results in $F_{14}(0, s) = 0$, $F_{24}(0, s) = 0$, and $F_{34}(0, s) = 0$, respectively.

(2) At $\zeta = L$, one can substitute $x_4(L, s) = 0$ in eq 23, which yields

$$x_4(0,\ s) = -\frac{1}{F_{44}(L,\ s)}\int_0^L \left[\frac{1}{\nu}F_{41}(L-\eta,\ s)x_1(\eta,\ 0) + \frac{1}{\nu}F_{42}(L-\eta,\ s)x_2(\eta,\ 0) + \frac{1}{\nu}F_{43}(L-\eta,\ s)x_3(\eta,\ 0) - \frac{1}{\nu_c}F_{44}(L-\eta,\ s)x_4(\eta,\ 0)d\eta\right] \tag{24}$$

Consequently, the resolvent operator can be determined utilizing eqs 23 and 24 in the following form

$$\begin{bmatrix} x_1(\zeta,\ s) \\ x_2(\zeta,\ s) \\ x_3(\zeta,\ s) \\ x_4(\zeta,\ s) \end{bmatrix} = \begin{bmatrix} \mathcal{R}_{11}(s,\ \mathcal{A}) & \mathcal{R}_{12}(s,\ \mathcal{A}) & \mathcal{R}_{13}(s,\ \mathcal{A}) & \mathcal{R}_{14}(s,\ \mathcal{A}) \\ \mathcal{R}_{21}(s,\ \mathcal{A}) & \mathcal{R}_{22}(s,\ \mathcal{A}) & \mathcal{R}_{23}(s,\ \mathcal{A}) & \mathcal{R}_{24}(s,\ \mathcal{A}) \\ \mathcal{R}_{31}(s,\ \mathcal{A}) & \mathcal{R}_{32}(s,\ \mathcal{A}) & \mathcal{R}_{33}(s,\ \mathcal{A}) & \mathcal{R}_{34}(s,\ \mathcal{A}) \\ \mathcal{R}_{41}(s,\ \mathcal{A}) & \mathcal{R}_{42}(s,\ \mathcal{A}) & \mathcal{R}_{43}(s,\ \mathcal{A}) & \mathcal{R}_{44}(s,\ \mathcal{A}) \end{bmatrix}\begin{bmatrix} x_1(\eta,\ 0) \\ x_2(\eta,\ 0) \\ x_3(\eta,\ 0) \\ x_4(\eta,\ 0) \end{bmatrix} \tag{25}$$

The associated resolvent operators can be expressed as

$$\begin{cases} \mathcal{R}_{i1}(s,\ \mathcal{A})(\cdot) = -\frac{F_{i4}(\zeta,\ s)}{F_{44}(L,\ s)}\int_0^L \frac{1}{\nu}F_{41}(L-\varepsilon,\ s)(\cdot)d\varepsilon + \int_0^\zeta \frac{1}{\nu}F_{i1}(\zeta-\eta,\ s)(\cdot)d\eta, & i = 1,\ 2,\ 3,\ 4 \\ \mathcal{R}_{i2}(s,\ \mathcal{A})(\cdot) = -\frac{F_{i4}(\zeta,\ s)}{F_{44}(L,\ s)}\int_0^L \frac{1}{\nu}F_{42}(L-\varepsilon,\ s)(\cdot)d\varepsilon + \int_0^\zeta \frac{1}{\nu}F_{i2}(\zeta-\eta,\ s)(\cdot)d\eta, & i = 1,\ 2,\ 3,\ 4 \\ \mathcal{R}_{i3}(s,\ \mathcal{A})(\cdot) = -\frac{F_{i4}(\zeta,\ s)}{F_{44}(L,\ s)}\int_0^L \frac{1}{\nu}F_{43}(L-\varepsilon,\ s)(\cdot)d\varepsilon + \int_0^\zeta \frac{1}{\nu}F_{i3}(\zeta-\eta,\ s)(\cdot)d\eta, & i = 1,\ 2,\ 3,\ 4 \\ \mathcal{R}_{i4}(s,\ \mathcal{A})(\cdot) = \frac{F_{i4}(\zeta,\ s)}{F_{44}(L,\ s)}\int_0^L \frac{1}{\nu_c}F_{44}(L-\varepsilon,\ s)(\cdot)d\varepsilon - \int_0^\zeta \frac{1}{\nu_c}F_{i4}(\zeta-\eta,\ s)(\cdot)d\eta, & i = 1,\ 2,\ 3,\ 4 \end{cases} \tag{26}$$

Now, the discrete-time operators in eq 18 can be solved by straightforwardly substituting the above-listed resolvent operators. Afterward, the discrete-time linear model is obtained as

$$X(\zeta,\ k) = \mathcal{A}_d X(\zeta,\ k-1) + \mathcal{B}_d u(k)$$
$$Y(k) = C_d X(\zeta,\ k-1) + \mathcal{D}_d u(k) \tag{27}$$

with the boundary conditions (eq 9) and the initial conditions (eq 10).

MPC Formulation. The formulation of the model predictive controller is developed for the discrete-time PDE model (eq 27). In particular, the constrained optimal controller design for the finite-dimensional system theory is extended and deployed for the infinite-dimensional system.

https://dx.doi.org/10.1021/acs.iecr.0c02500
Ind. Eng. Chem. Res. 2020, 59, 18921−18936

Two cases are used to demonstrate the performance of the controller: the first case includes the state feedback MPC with the assumption that full states are available and the second one is a Luenberger observer-based MPC to reconstruct the state from the available output measurements. These two cases are shown schematically in Figure 3. One can note that, in the MPC formulation, the state and the output are denoted $Z(\zeta, k)$ and $V(k)$, respectively, to avoid confusion in the notation.

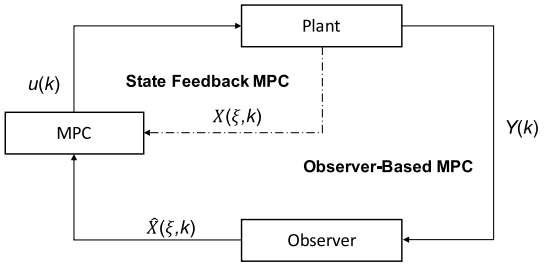

Figure 3. Scheme of state-feedback MPC and observer-based MPC.

State-Feedback MPC. In this section, the MPC design for the finite-dimensional system is extended to the discrete-time infinite-dimensional tubular reactor model based on the previous contributions.[9,36,49] The predictive controller is found as the solution of an optimization problem such that the following open-loop objective function on an infinite horizon is minimized at a given sampling time k

$$\min_{u^N} \sum_{j=0}^{\infty} V_{k+j|k}^{\mathrm{T}} Q V_{k+j|k} + u_{k+j|k}^{\mathrm{T}} R u_{k+j|k} + \Delta u_{k+j|k}^{\mathrm{T}} \bar{S} \Delta u_{k+j|k} \tag{28}$$

where Q is a symmetric positive semidefinite spatial operator and R is a symmetric positive definite spatial operator. $V_{k+j|k}$ and $u_{k+j|k}$ represent the output and input variables at future time $k + j$ predicted at current time k and the term $\Delta u_{k+j|k}$ denotes the change in an input vector at time $k + j$ as $\Delta u_{k+j|k} = u_{k+j|k} - u_{k+j-1|k}$. The vector u^N includes the control sequence $\{u_{k|k}, u_{k+1|k}, u_{k+2|k}, \cdots, u_{k+N-1|k}\}$ and the first element $u_{k|k}$ will be injected to the plant as the future control action.

A typical feature in MPC is that the infinite-horizon objective function can be cast into a finite-horizon objective function by assuming that the inputs are zero beyond the control horizon N, that is, $u_{k+N|k} = 0$, $j \geq N$. In addition, one penalty term needs to be added to the objective function in order to approximate the inputs and outputs beyond the horizon.[50] In this case, under the assumption of observability, the terminal output penalty term can be written as the corresponding state penalty term. As the state is a spatio-temporal variable, the penalty term is given in the form of the inner product. Therefore, the finite horizon objective function with input and output constraints can be formulated as follows

$$\min_{u^N} \sum_{j=0}^{N-1} V_{k+j|k}^{\mathrm{T}} Q V_{k+j|k} + u_{k+j|k}^{\mathrm{T}} R u_{k+j|k} + \langle Z_{k+N-1|k}, \bar{Q} Z_{k+N-1|k} \rangle$$

s.t.

$$Z_{\zeta, k-1|k} = X_{\zeta, k-1|k}$$

$$Z_{k+j|k} = \mathcal{A}_{\mathrm{d}} Z_{k+j-1|k} + \mathcal{B}_{\mathrm{d}} u_{k+j|k}$$

$$V_{k+j|k} = C_{\mathrm{d}} Z_{k+j-1|k} + \mathcal{D}_{\mathrm{d}} u_{k+j|k}$$

$$u_{\min} \leq u_{k+j|k} \leq u_{\max}$$

$$V_{\min} \leq V_{k+j|k} \leq V_{\max} \tag{29}$$

where N is the prediction horizon, $\bar{Q}$ is the spatial operator to penalize the terminal state which depends on the stability of the given model. $u_{\min}$ and $u_{\max}$ are the lower and upper bound vectors of the manipulated input $u(t)$. Moreover, $V_{\min}$ and $V_{\max}$ are lower and upper output constraints, respectively. It is important to note that the input and output constraints are imposed for two fundamentally different reasons. The input constraint usually represents physical limits of the control actuator or available control actuation, such as the limitation of the flow valve. For the output constraint, it usually represents the typical requirements among the operation of tubular reactors in practice, such as the temperature of product not exceeding certain ranges, as well as the physical limits of actuators or sensors.

According to the nature of transport reaction systems, one can define $\bar{Q}$ as the infinite sum $\bar{Q} = \sum_{i=0}^{\infty} \mathcal{A}_{\mathrm{d}}^{*i} C_{\mathrm{d}}^{*} Q C_{\mathrm{d}} \mathcal{A}_{\mathrm{d}}^{i}$, which can be determined from the solution of the following discrete Lyapunov equation[50]

$$\mathcal{A}_{\mathrm{d}}^{*} \bar{Q} \mathcal{A}_{\mathrm{d}} + C_{\mathrm{d}}^{*} Q C_{\mathrm{d}} = \bar{Q} \tag{30}$$

In particular, it can be demonstrated that the unique solution of the discrete Lyapunov equation is directly related to the continuous one, which is shown as follows[48]

$$\mathcal{A}^{*} \bar{Q} + \bar{Q} \mathcal{A} = -C^{*} Q C \tag{31}$$

The assumption of C being infinite-time admissible for $\mathcal{A}$ is required which denotes the continuous-time Lyapunov equation having solutions.[51] By multiplying a spatial function $X(\zeta)$ and substituting the operator $\mathcal{A}$ on both sides, we can obtain

$$\mathcal{A}^{*} \bar{Q} X + \bar{Q} \mathcal{A} X = -C^{*} Q C X$$

$$-V \frac{\partial \bar{Q} X}{\partial \zeta} + \mathcal{A}^{\mathrm{T}} \bar{Q} X + \bar{Q} \left(V \frac{\partial X}{\partial \zeta} + \mathcal{A} X \right) = -C^{*} Q C X$$

$$-V \bar{Q} \frac{\partial X}{\partial \zeta} - V \frac{\partial \bar{Q}}{\partial \zeta} X + \mathcal{A}^{\mathrm{T}} \bar{Q} X + V \bar{Q} \frac{\partial X}{\partial \zeta} + \bar{Q} \mathcal{A} X = -C^{*} Q C X$$

$$\frac{\partial \bar{Q}}{\partial \zeta} = V^{-1} \mathcal{A}^{\mathrm{T}} \bar{Q} + V^{-1} \bar{Q} \mathcal{A} + V^{-1} C^{*} Q C$$

where $\bar{Q} \in \mathcal{D}(\mathcal{A}^{*})$. As a result, the straightforward algebraic manipulation of the objective function presented in eq 29 leads to the following quadratic programming optimization problem.

https://dx.doi.org/10.1021/acs.iecr.0c02500
Ind. Eng. Chem. Res. 2020, 59, 18921−18936

$$\min_U J = \frac{1}{2}U^T H U + U^T \langle I,\ F Z_{\zeta,\,k-1|k}\rangle + \langle Z_{\zeta,\,k-1|k},\ \bar{Q} Z_{\zeta,\,k-1|k}\rangle$$

s.t.

$$U_{\min} \le U \le U_{\max}$$

$$V_{\min} \le GU + S Z_{\zeta,\,k-1|k} \le V_{\max} \tag{32}$$

where $U = \{u_{k+n}\}_{n=1}^{N}$ and $H \in \mathcal{L}(U)$ are positive and self-adjoint, respectively. By direct calculation, it is straightforward to find

$$h_{i,j} = \begin{cases} \mathcal{D}_d^* Q \mathcal{D}_d + \mathcal{B}_d^* \bar{Q} \mathcal{B}_d + R & \text{for } i = j \\ \mathcal{D}_d^* Q C_d \mathcal{A}_d^{\,i-j-1} \mathcal{B}_d + \mathcal{B}_d^* \bar{Q} \mathcal{A}_d^{\,i-j} \mathcal{B}_d & \text{for } i > j \\ h_{j,i}^* & \text{for } i < j \end{cases} \tag{33}$$

with F given by $F = \{\mathcal{D}_d^* Q C_d \mathcal{A}_d^{\,k-1} + \mathcal{B}_d^* \bar{Q} \mathcal{A}_d^{\,k}\}_{k=1}^{N-1}$.

The constraints of eq 32 can be written in the form

$$\begin{bmatrix} I \\ -I \\ G \\ -G \end{bmatrix} U \le \begin{bmatrix} U_{\max} \\ -U_{\min} \\ V_{\max} - S Z_{\zeta,\,k-1|k} \\ -V_{\min} + S Z_{\zeta,\,k-1|k} \end{bmatrix} \tag{34}$$

where G is a lower triangular matrix given by

$$g_{i,j} = \begin{cases} \mathcal{D}_d & \text{for } i = j \\ C_d \mathcal{A}_d^{\,i-j-1} \mathcal{B}_d & \text{for } i > j \\ 0 & \text{for } i < j \end{cases}$$

and $S = \{C_d \mathcal{A}_d^{\,k-1}\}_{k=1}^{N}$.

Observer-Based MPC. In the previous section, we assumed that the states are available at each sample time k. In other words, it requires knowledge of the current state of the system in order to compute the solution of optimal input formulated at each interval. However, in most applications, state information is not always known. Therefore, for output feedback, a Luenberger observer which can reconstruct the states based on the output measurements is needed. In general, there are two ways to design the Luenberger observer, including the continuous-time observer based on the continuous system model and the discrete one under the discrete setting.

First, let us recall the linearized continuous-time model

$$\dot{X}(\zeta,\ t) = \mathcal{A} X(\zeta,\ t) + \mathcal{B} u(t)$$
$$Y(t) = C X(\zeta,\ t) \tag{35}$$

The Luenberger observer is presented by the following equations

$$\dot{\hat{X}}(\zeta,\ t) = \mathcal{A} \hat{X}(\zeta,\ t) + \mathcal{B} u(t) + L_c(Y(t) - \hat{Y}(t))$$
$$\hat{Y}(t) = C \hat{X}(\zeta,\ t) \tag{36}$$

where L_c is the continuous observer gain to be designed. Stability of the observer implies that the state estimation error, $e(\zeta,\ t) = X(\zeta,\ t) - \hat{X}(\zeta,\ t)$, converges to zero as time increases. The error dynamic equation is shown as follows

$$\dot{e}(\zeta,\ t) = (\mathcal{A} - L_c C) e(\zeta,\ t) \tag{37}$$

The design problem can be formulated as the choice of the gain L_c such that the error dynamic eq 37 has exponential stability. Therefore, if $\mathcal{A} - L_c C$ can generate an exponentially stable C_0 semigroup, then the error e converges exponentially to zero as $t \to \infty$.[48] Based on this consideration, the following Lyapunov type of argument is introduced that can be applied in the design of the L_c operator and, here, we denote $\mathcal{A}_c = \mathcal{A} - L_c C$.

Let $\mathcal{A}_c$ be an infinitesimal generator of the C_0-semigroup $\mathcal{T}_{\mathcal{A}_c}(t)$ on the Hilbert space and M be a positive operator. Then, the $\mathcal{T}_{\mathcal{A}_c}(t)$ is exponentially stable if and only if there exists a nonnegative self-adjoint operator Q_c as a solution of the following operator Lyapunov equation such that

$$\langle Q_c X,\ \mathcal{A}_c^* X\rangle + \langle \mathcal{A}_c^* X,\ Q_c X\rangle = -\langle MX,\ X\rangle,\ X \in \mathcal{D}(\mathcal{A}_c^*) \tag{38}$$

holds and where M is the positive definite design parameter and Q_c is a nonnegative self-adjoint operator which maps from $\mathcal{D}(\mathcal{A}_c^*)$ to $\mathcal{D}(\mathcal{A}_c)$. However, eq 38 is difficult to solve because both of the operators Q_c and L_c need to be determined. Considering the error dynamic $\mathcal{A} - L_c C$ can be arbitrarily selected by choosing the observer gain L_c suitably when the observability condition holds,[52] one can assume $L_c = Q_c C^*$, and then the Lyapunov equation can be transformed into the operator Riccati equation as follows.

Let us assume that the pair $(\mathcal{A},\ C)$ is exponentially detectable, then there exists a nonnegative self-adjoint operator Q_c which is the solution of the following operator Riccati equation[53,54]

$$\mathcal{A} Q_c + Q_c \mathcal{A}^* - 2 Q_c C^* C Q_c + M = 0, \qquad \text{on } \mathcal{D}(\mathcal{A}^*) \tag{39}$$

with $Q_c(\mathcal{D}(\mathcal{A}_c^*)) \subset \mathcal{D}(\mathcal{A}_c)$. The observer gain $L_c = Q_c C^*$ is an exponentially stabilizing gain which guarantees the exponential stability of $\mathcal{A}_c = \mathcal{A} - L_c C$. In addition, by adjusting M proportionally, we can design a desired observer gain that results in the desired convergency rate of error dynamic.[54]

In a similar manner, one can design a discrete Luenberger observer based on the following discrete-time model

$$X(\zeta,\ k) = \mathcal{A}_d X(\zeta,\ k-1) + \mathcal{B}_d u(k)$$
$$Y(k) = C_d X(\zeta,\ k-1) + \mathcal{D}_d u(k) \tag{40}$$

The observer is constructed by the following equations

$$\hat{X}(\zeta,\ k) = \mathcal{A}_d \hat{X}(\zeta,\ k-1) + \mathcal{B}_d u(k) + L_d(Y(k) - \hat{Y}(k))$$
$$\hat{Y}(k) = C_d \hat{X}(\zeta,\ k-1) + \mathcal{D}_d u(k) \tag{41}$$

where L_d is the discrete observer gain to be designed. Similarly, we can obtain the error dynamic as $e_k = (\mathcal{A}_d - L_d C_d) e_{k-1}$. To obtain a stabilizing observer gain, one can find the nonnegative self-adjoint operator Q_d by solving the following Discrete Lyapunov equation

https://dx.doi.org/10.1021/acs.iecr.0c02500
Ind. Eng. Chem. Res. 2020, 59, 18921−18936

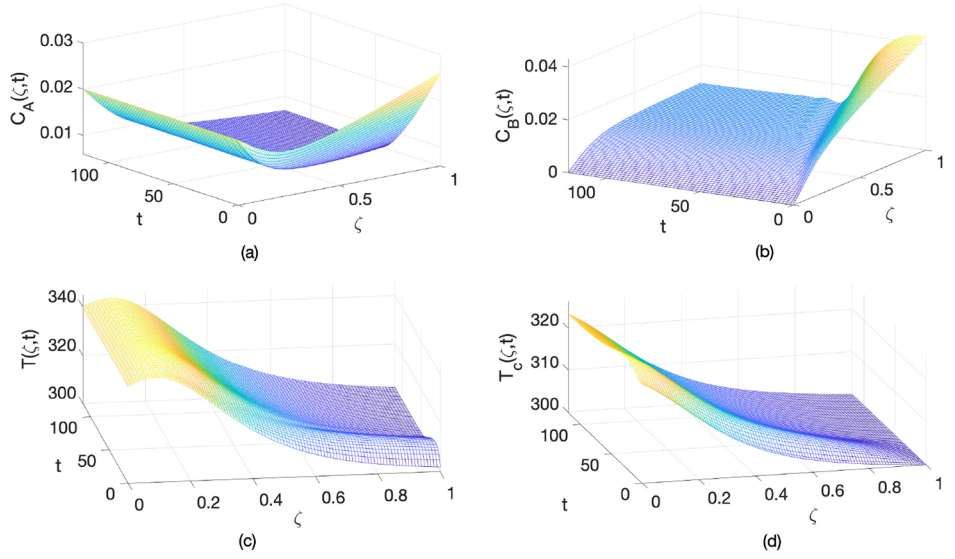

Figure 4. Open-loop steady-state profiles of the tubular reactor.

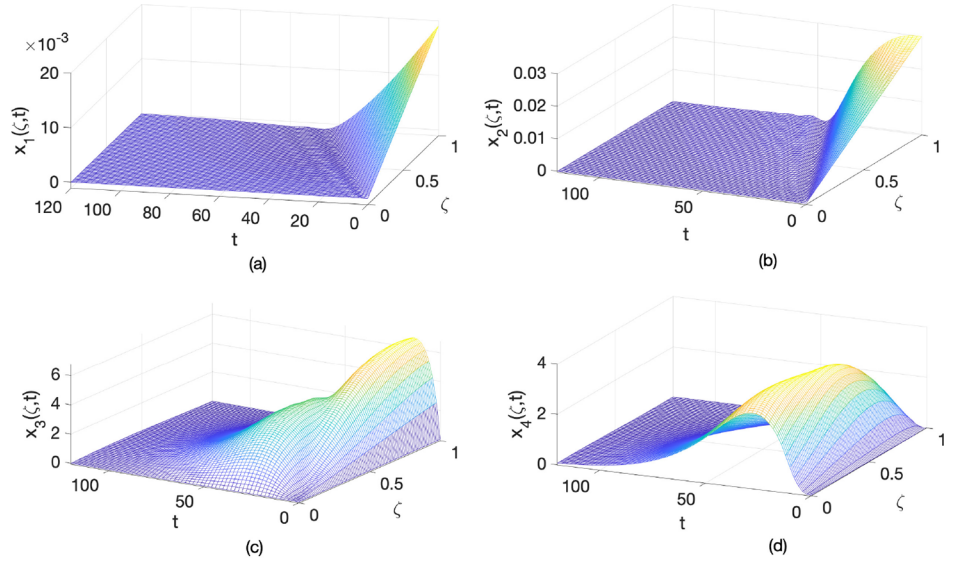

Figure 5. Perturbations of open-loop-state profiles of the tubular reactor from eq 27.

$$\langle X,\ [\tilde{\mathcal{A}}_d^* Q_d \tilde{\mathcal{A}}_d - Q_d]X\rangle = -\langle X,\ [\tilde{C}_d^* N \tilde{C}_d]X\rangle \tag{42}$$

where $\tilde{\mathcal{A}}_d = \mathcal{A}_d - L_d C_d = -I(\cdot) + 2\delta[\delta I - \mathcal{A}_c]^{-1}$ and $\tilde{C}_d = \sqrt{2\delta}C[\delta - \tilde{\mathcal{A}}_d]^{-1}$. It can be demonstrated that the solution of the discrete Lyapunov equation is also the solution of the continuous Lyapunov equation under the Cayley–Tustin time-discretization setting.[53,55] Therefore, the discrete Luenberger observer gain can be obtained by constructing the continuous observer gain.

According to the principle of predictive control, the state estimated by the observer at the current moment will be used as the starting point for predicting the future dynamics of the system. Hence, the observer-based MPC can be reconstructed by setting the initial state equal to the estimate of the current state at each time k, that is, $Z_{\zeta,\,k-1|k} = \hat{X}_{\zeta,\,k-1|k}$. One can obtain the estimate of the current state from the Luenberger observer, from which one can reconstruct the entire state trajectory.[56] In this case, the observer-based MPC is directly formulated as follows

$$\begin{aligned}
&\min_{u^N} \sum_{j=0}^{N-1} V_{k+j|k}^{\mathrm{T}} Q V_{k+j|k} + u_{k+j|k}^{\mathrm{T}} R u_{k+j|k} + \langle Z_{k+N-1|k},\ \bar{Q} Z_{k+N-1|k}\rangle \\
&\text{s.t.} \\
&Z_{\zeta,\,k-1|k} = \hat{X}_{\zeta,\,k-1|k} \\
&Z_{k+j|k} = \mathcal{A}_d Z_{k+j-1|k} + \mathcal{B}_d u_{k+j|k} \\
&V_{k+j|k} = C_d Z_{k+j-1|k} + \mathcal{D}_d u_{k+j|k} \\
&u_{\min} \le u_{k+j|k} \le u_{\max},\ V_{\min} \le V_{k+j|k} \le V_{\max}
\end{aligned} \tag{43}$$

where u^N, N, Q, R, and $\bar{Q}$ are as in eq 29. As for implementation, the Luenberger observer design and MPC must be performed iteratively until the performance is acceptable.

Simulation Study. In this section, the performance of the two MPC formulations developed in the previous section is demonstrated through two case studies. Case study 1 illustrates the state-feedback MPC design, where all states of the system are assumed to be available or measurable. The sensitivity

https://dx.doi.org/10.1021/acs.iecr.0c02500
Ind. Eng. Chem. Res. 2020, 59, 18921−18936

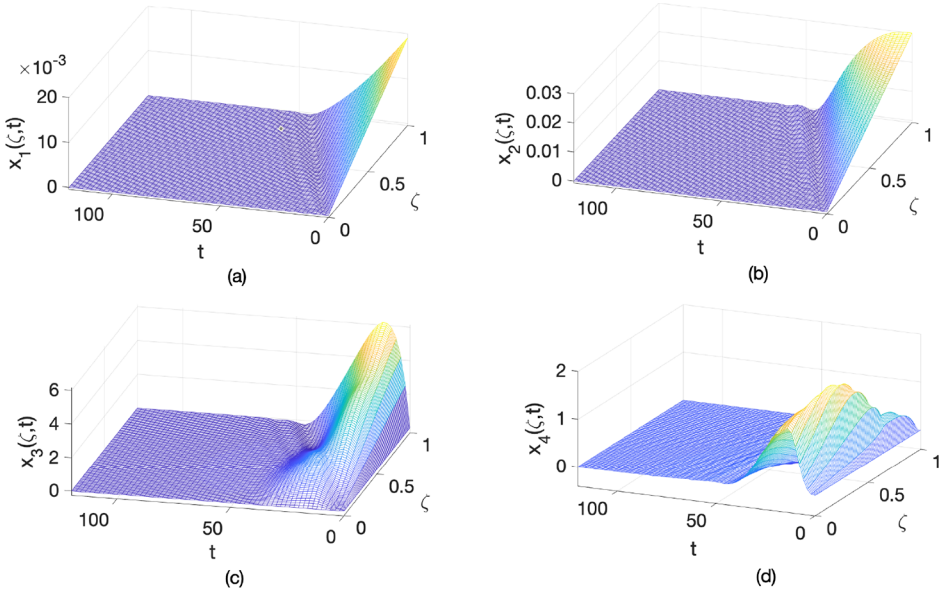

Figure 6. Perturbations of closed-loop state profiles of the tubular reactor under the state-feedback MPC law from eq 32.

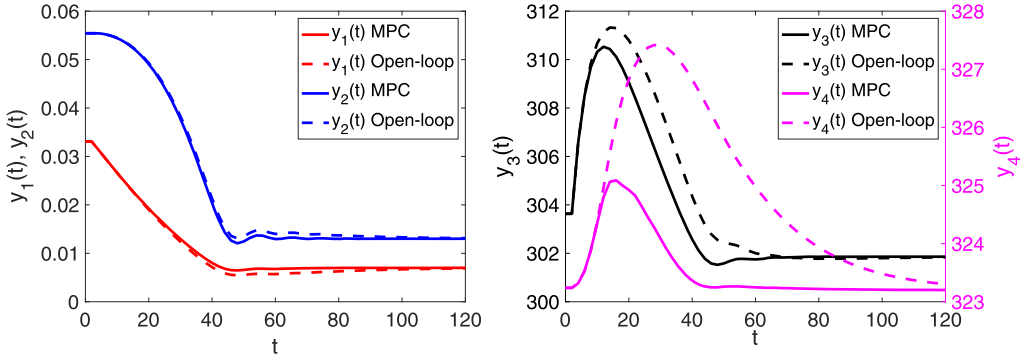

Figure 7. Performance comparison of open-loop and closed-loop output profiles under the state-feedback MPC law from eq 32.

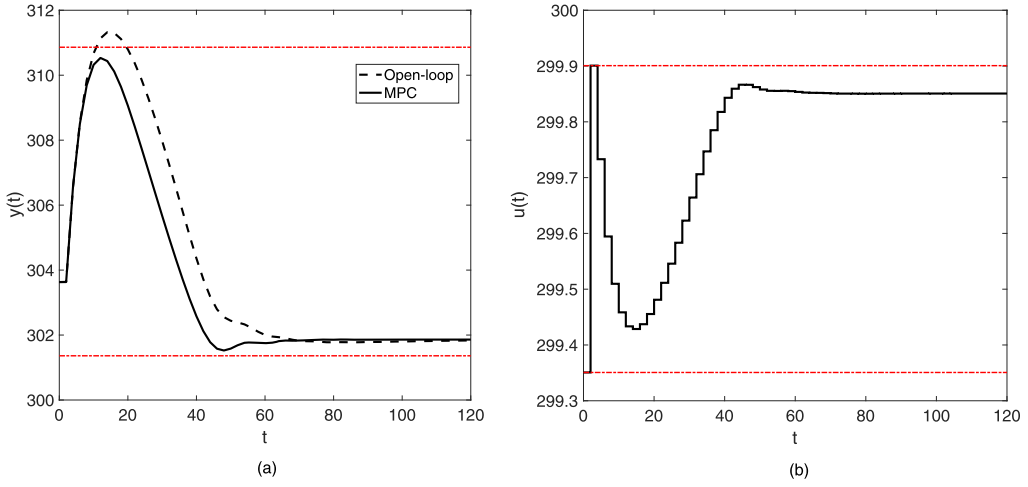

Figure 8. (a) Comparison between profiles of the open-loop and closed-loop outputs (y_3) using the state-feedback MPC from eq 32. (b) Input profile calculated in the state-feedback MPC case from eq 32.

analysis of input and output weights and constraints of MPC formulation is given. Considering the unavailability of state measurements in realistic tubular reactors, the observer is designed to reconstruct the states, based on which an observer-based MPC is simulated as Case study 2. Both of the controllers are designed to satisfy the input and output constraint requirements and achieve system stabilization at the same time. The resulting constrained optimization problems become quadratic-programing problems, which are solved using the MATLAB subroutine QuadProg.

https://dx.doi.org/10.1021/acs.iecr.0c02500
Ind. Eng. Chem. Res. 2020, 59, 18921−18936

Table 2. Performance Comparison of the State-Feedback MPC with Different Input and Output Weights and Constraints

weights		+10%	+5%	base case	−5%	−10%
Q = diag{0.5, 0.5,0.5, 0.5}	R = 5	1.00×10^{-3}	1.00×10^{-3}	1.00×10^{-3}	7.91×10^{-4}	4.46×10^{-5}
	R = 10	5.03×10^{-3}	5.03×10^{-3}	5.03×10^{-3}	4.51×10^{-3}	3.51×10^{-3}
Q = diag{5,5,5,5}	R = 5	1.32×10^{-3}	1.51×10^{-3}	1.67×10^{-3}	1.83×10^{-3}	2.14×10^{-3}
	R = 10	5.71×10^{-4}	8.53×10^{-4}	8.79×10^{-4}	9.95×10^{-4}	1.77×10^{-3}

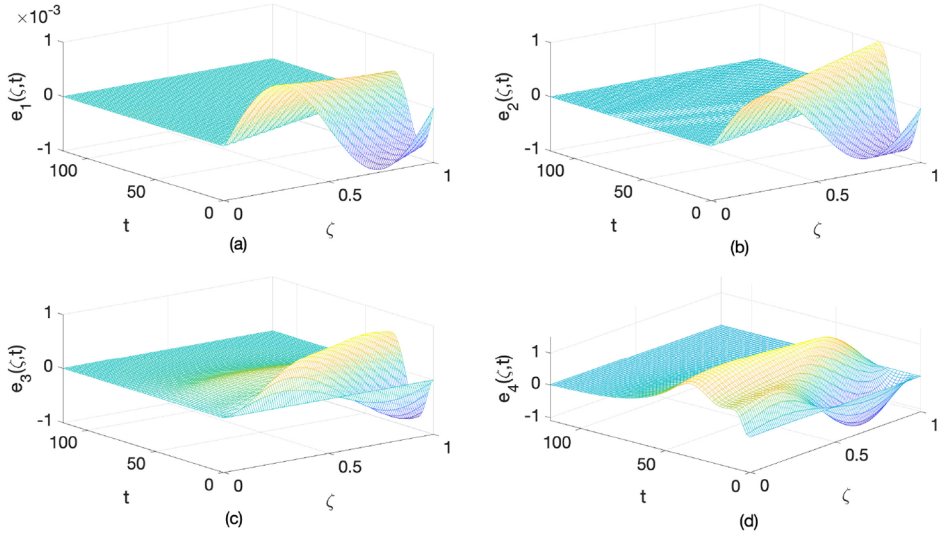

Figure 9. Evolution of the observer error $e(\zeta, t)$.

The parameter values used in eq 32 and for simulations are listed in Table 1. For the initial conditions of the dynamic system, we consider $x_1(\zeta, 0) = 0.019\ \zeta$, $x_2(\zeta, 0) = 0.03\ \zeta$, $x_3(\zeta, 0) = 0.02\ \zeta$, $x_4(\zeta, 0) = 0.02(1 - \zeta)$. In addition, $\overline{\zeta}_L = 0.15$ is chosen for the input operator. In both cases, the horizon of $N = 15$ is selected with the terminal constraint formulation. The input and output weights are chosen as $R = 5$ and $Q = \text{diag}\{0.5, 0.5, 0.5, 0.5\}$ for MPC implementation, respectively. The input and output constraints are considered as $u_{min} = -0.5$, $u_{max} = 0.05$, $V_{min} = -0.5$, and $V_{max} = 9$ with respect to state perturbation. As for the Cayley−Tustin time discretization, we choose $h = 2$ at the time discretization interval, which implies $\delta = 1$. The spatial discretization interval is taken as $d\zeta = 0.01$.

As shown in Figure 4, the open-loop states converge to their corresponding steady states rapidly which indicates that the original plant is intrinsically stable. By implementing the proposed MPC frameworks, we aim to steer the convergence rate without violating the physical constraints of actuators and sensors. In order to clearly show the perturbation of each state, the linearized states are depicted in Figure 5, where it is apparent that all states go close to zero within the considered time range.

Case Study 1: State-Feedback MPC. By implementing the optimal control input on the plant model, the states of the closed-loop system under the MPC law given by eq 32 are obtained and shown in Figure 6. The closed-loop system is stabilized because all of the states go to zero with a faster convergence rate compared with the open-loop states shown in Figure 5. This can also be verified from the output profiles shown in Figure 7, where the four outputs under the state-feedback MPC law converge to steady states which are faster than the corresponding open-loop profiles. In this case, we aim to steer the temperature of the reactor without exceeding its corresponding physical constraint. It can be observed from Figure 8a that, compared with the open-loop temperature profiles, the closed-loop profile converge to a steady state at a faster rate and satisfy the constraints simultaneously. The corresponding manipulated input is given in Figure 8b. The control effort is required on the half of the time horizon to keep the output inside the range of set limits and, after that, the requirement for input control is not obvious.

In addition, the influence of the choice of the input and output weights (Q and R) on the state-feedback MPC performance is investigated below, where the average absolute error is taken as the evaluation index. With the same objective function and horizon, different input and output constraints (with ±5 and ±10% based on the chosen case $u_{min} = -0.5$, $u_{max} = 0.05$, $V_{min} = -0.5$, and $V_{max} = 9$) are implemented. As illustrated in Table 2, it is apparent that the state-feedback MPC generally presents a very small average absolute error which stays within a reasonable range (4.46×10^{-5} to 1.00×10^{-3}) under these conditions considered. In particular, when the input and output weights are chosen as $R = 5$ and $Q = \text{diag}\{0.5, 0.5, 0.5, 0.5\}$ for MPC implementation, the average absolute error is the smallest and is the case considered in this article.

Case Study 2: Observer-Based MPC. The performance of observer-based MPC is now described. Compared with the implementation of the state-feedback MPC, the MPC is now implemented based on the estimate states. First, in order to obtain the estimate states, the observer design implies that the expression in eq 39 is applied, with an arbitrary choice of the design parameter $M(\zeta)$ and $\Psi(\zeta)$ in the domain of $\mathcal{D}(\mathcal{A}^*)$, which leads to the following equations

https://dx.doi.org/10.1021/acs.iecr.0c02500
Ind. Eng. Chem. Res. 2020, 59, 18921−18936

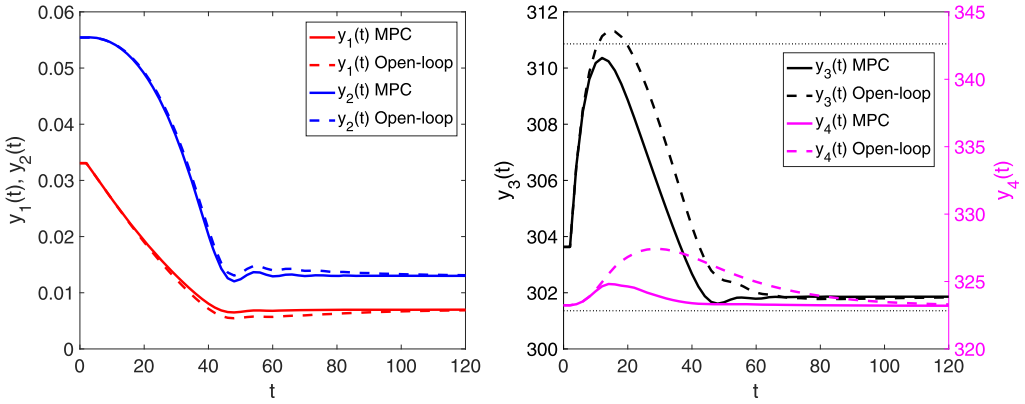

Figure 10. Performance comparison of open-loop and closed-loop output profiles under the observer-based MPC law from eq 43.

$$\mathcal{A}Q_c\Psi(\zeta) + Q_c\mathcal{A}^*\Psi(\zeta) + M\Psi(\zeta) - 2Q_cC^*CQ_c\Psi(\zeta) = 0$$

$$V\frac{\partial Q_c}{\partial \zeta}\Psi(\zeta) + VQ_c\frac{\partial \Psi}{\partial \zeta} + A(\zeta)Q_c\Psi(\zeta) + Q_c\left[-V\frac{\partial \Psi}{\partial \zeta} + A(\zeta)^*\Psi(\zeta)\right] + M\Psi(\zeta) - 2Q_cC^*CQ_c\Psi(\zeta) = 0$$

$$V\frac{\partial Q_c}{\partial \zeta}\Psi(\zeta) + A(\zeta)Q_c\Psi(\zeta) + Q_cA(\zeta)^*\Psi(\zeta) + M\Psi(\zeta) - 2Q_cC^*CQ_c\Psi(\zeta) = 0$$

which yields

$$\frac{dQ_c}{d\zeta} = V^{-1}[2Q_cC^*CQ_c - 2A(\zeta)Q_c - M] \quad (44)$$

Therefore, one needs to choose Q_c, which in the domain of $\mathcal{A}$ and positive function M ensure the nonnegative definiteness of Q_c. Choosing M to be 0.001, Q_c can be solved numerically and then the observer gain is found to be $L = Q_cC^*$. As shown in Figure 9, the estimation error of the designed Luenberger observer converges to zero with increasing time.

As shown in Figure 10, the output profiles under the observer-based MPC law converge to steady states that are similar to the corresponding state-feedback output profiles, as shown in Figure 7. The third output under the observer-based MPC law has a faster convergency rate than the open-loop profile. The obvious difference between them is that the observer-based MPC keeps the output within the given constraints to satisfy the requirements. The input manipulation obtained from the observer-based MPC, which is the solution of the constrained optimization problem in eq 43, is shown in Figure 11. The comparison of plant outputs and observer outputs is shown in Figure 12. The estimated outputs have a slight overshoot compared with plant outputs, but there are no obvious differences in terms of convergency rates.

In order to further investigate the performance of the proposed MPC design, we consider two truly unknown disturbances which make the open-loop system potentially unstable. In addition, we assumed that the addition of disturbance does not affect the feasibility of input and output constraints. Specifically, two types of disturbances, including

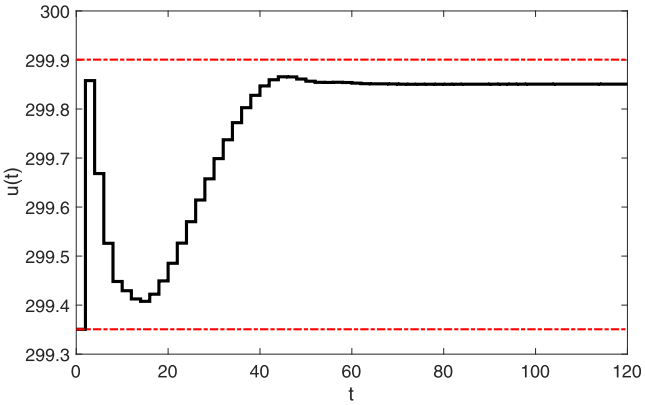

Figure 11. Input profile computed by the observer-based MPC in eq 43.

the input disturbance and the distributed disturbance, were injected into the system.

In this first scenario, we consider the input disturbance, $d(t) = 0.0005\ \sin(0.06t)$. The perturbations of open-loop-state profiles shown in Figure 13 have shown the sinusoidal trend given by the disturbance signal considered here, and the proposed MPC design can stabilize the unstable modes, as illustrated in Figure 14. As shown in Figure 15, it is apparent that the open-loop output responses oscillate due to input disturbance injection. The MPC controller is able to simultaneously realize disturbance rejection and converge to steady states in a short time and satisfies the given constraints. The corresponding manipulated input is given in Figure 16. Therefore, it can be clearly seen that under the consideration of input disturbance, the proposed MPC achieves good control performance.

In this second scenario, we consider the distributed disturbance which is expressed by a step signal, $d(t) = \begin{cases} 0.0001, & t \in [32, 62] \\ 0 & \text{otherwise} \end{cases}$. As shown in Figure 17, the open-loop outputs show significant oscillation when the step disturbance is applied. The closed-loop output profiles show that the disturbance does not affect the designed control law because of the fast convergency rate and good disturbance rejection. The corresponding manipulated input is given in Figure 18. It is apparent that the control actions become more reliable and the system converges faster.

Finally, the performances of open-loop, state-feedback MPC and observer-based MPC are compared from the perspectives

https://dx.doi.org/10.1021/acs.iecr.0c02500
Ind. Eng. Chem. Res. 2020, 59, 18921−18936

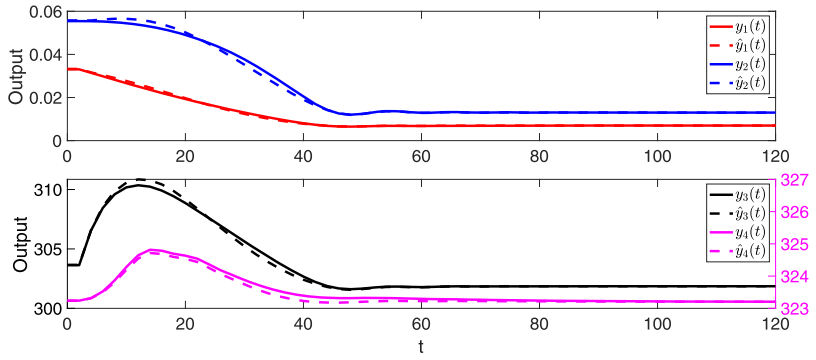

Figure 12. Estimated output profiles using the Luenberger observer.

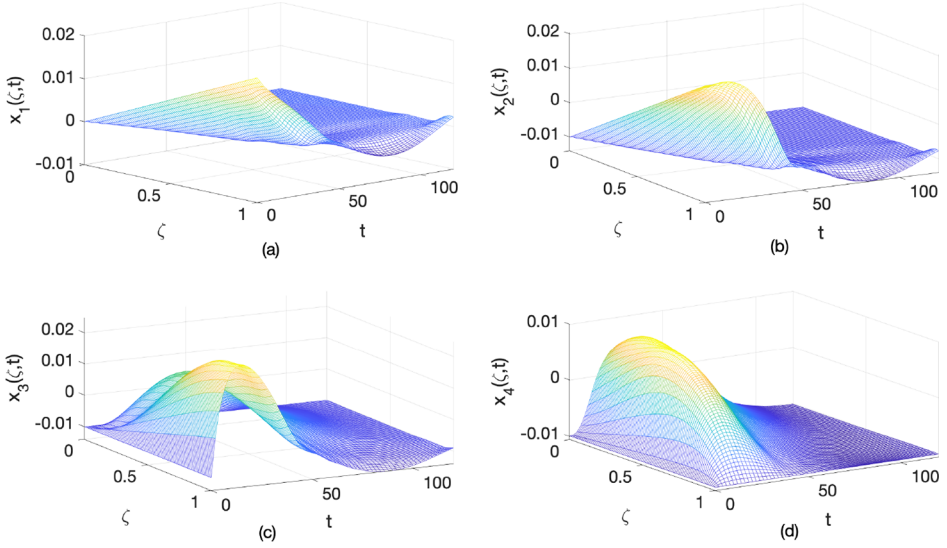

Figure 13. Perturbations of open-loop-state profiles under the consideration of input disturbance.

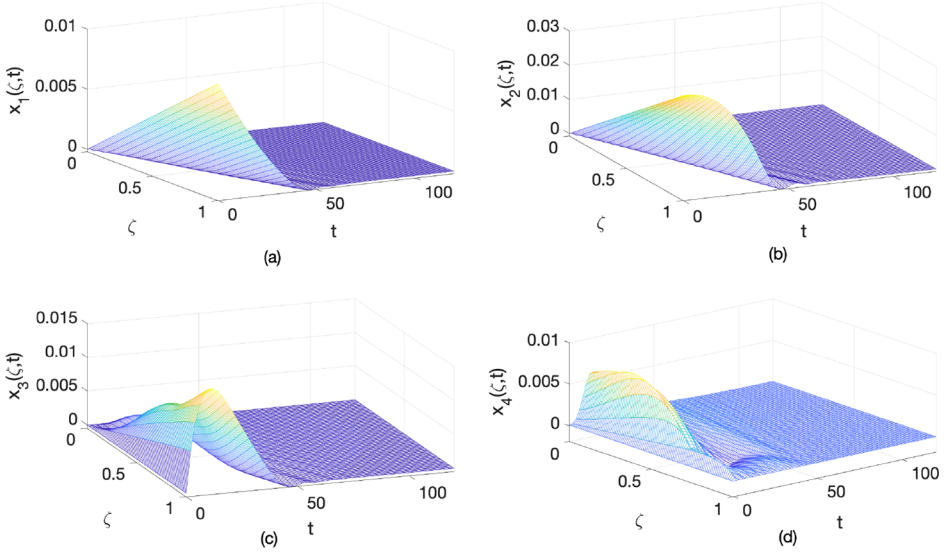

Figure 14. Perturbations of closed-loop-state profiles under the consideration of input disturbance with the observer-based MPC law from eq 43.

of average settling time and absolute error under the consideration of two types of disturbances with the same overall simulation time of 120 s. More specifically, the settling time is calculated as the time taken by the output response to reach the steady states with 2% tolerance in this case. The absolute error is defined as the absolute difference in the controlled outputs and the outputs according to steady states at 120 s. The average settling time and absolute error are calculated by taking average of all outputs. For the disturbance signals, we consider two same types of disturbances including the input disturbance and the distributed disturbance.

https://dx.doi.org/10.1021/acs.iecr.0c02500
Ind. Eng. Chem. Res. 2020, 59, 18921−18936

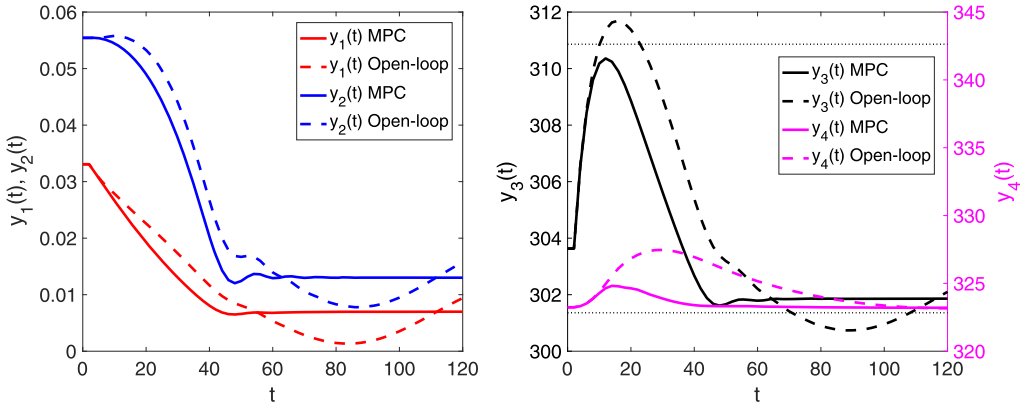

Figure 15. Closed-loop output profiles under the consideration of input disturbance with the observer-based MPC law from eq 43.

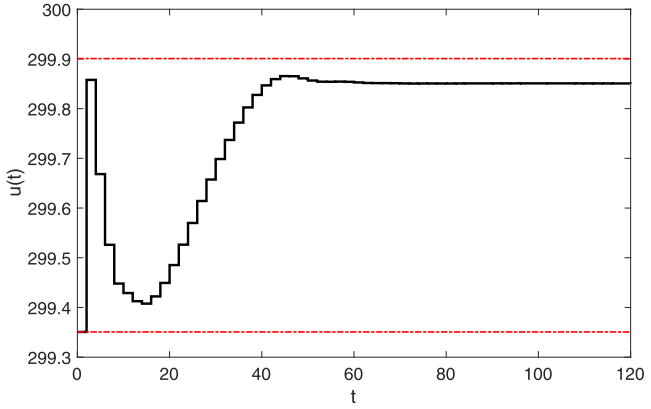

Figure 16. Input profile calculated in the observer-based MPC case from eq 43.

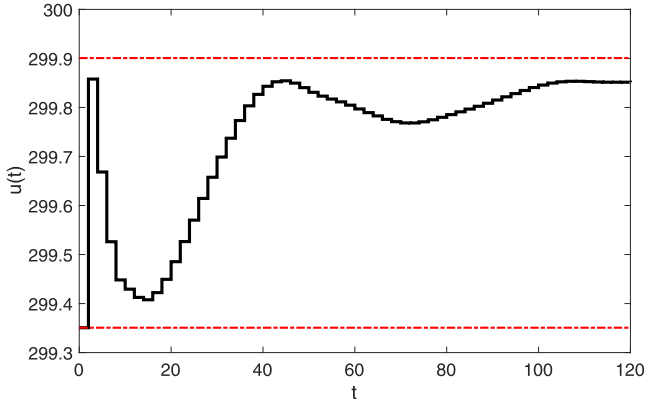

Figure 18. Input profile generated by the observer-based MPC from eq 43.

As illustrated in Table 3, it is apparent that the settling time of state-feedback MPC is slightly smaller than the observer-based MPC under the consideration of input sinusoidal disturbance, while for the open-loop system, the settling time is not achieved during the overall simulation. The average absolute error of the open-loop system is 5.13×10^{-2}, which is worse than the error of two strategy controller (9.75×10^{-4} and 3.73×10^{-4}, respectively), where the observer-based MPC shows a competitive performance to the state-feedback MPC. Under the proposed distributed disturbance consideration, the overall trend is similar to the input disturbance, but the open-loop system shows a worse absolute error than other cases. Through simulation studies, it can be seen that the feasibility

Table 3. Performance Comparison of Open-Loop and Closed-Loop Systems with Different Types of Disturbances

types of disturbances	input disturbance		distributed disturbance	
specifications	settling time (s)	absolute error	settling time (s)	absolute error
open-loop		5.13×10^{-2}	75.5	1.10
state-feedback MPC	42	3.73×10^{-4}	67	4.33×10^{-3}
observer-based MPC	45	9.75×10^{-4}	68	4.93×10^{-3}

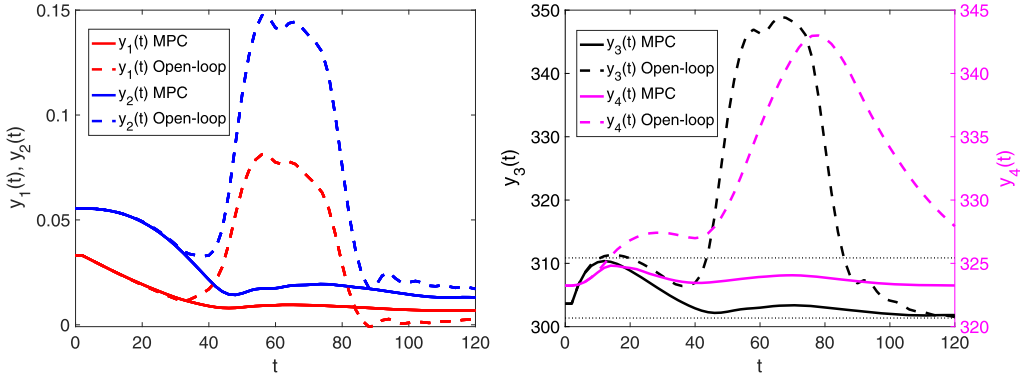

Figure 17. Closed-loop output profiles considering the distributed disturbance under the observer-based MPC law from eq 43.

https://dx.doi.org/10.1021/acs.iecr.0c02500
Ind. Eng. Chem. Res. 2020, 59, 18921−18936

and applicability for the MPC design are valid. As expected, the two constrained predictive controllers developed in this work are able to minimize the energy cost and/or prevent damage to equipment (sensors and actuators) in order to improve the safety and efficiency of the system.

The novelty of the proposed design method lies in the combination of Cayley−Tustin time discretization of the PDE model with MPC application in the tubular reactor with a reversible reaction. Therefore, the proposed design outperforms other numerical simulation methods using Cayley−Tustin time discretization because of the numerical stability, energy-preserving, and theoretical properties (such as stability, controllability, and observability) preserved in a late lumping manner. The construction of the model predictive controller of an infinite-dimensional system leads to a finite-dimensional constrained quadratic optimization problem which is easily solvable using standard numerical optimization methods.

CONCLUSIONS

In summary, the MPC algorithms are developed in this work for a jacket tubular reactor as the distributed parameter system, considering the input and state constraints. The plant is described by a set of nonlinear coupled hyperbolic PDEs considering a simple reversible exothermic reaction taking place in the reactor ($A \rightleftharpoons B$). In particular, a spatially varying jacket temperature is considered in this work instead of a constant one. After applying linearization around a given equilibrium operating point of interest, a linearized PDE model is obtained for modeling tubular reactor dynamics. For model time-discretization, the Cayley−Tustin transform is utilized to map the continuous-time system to the discrete-time model representation without spatial discretization and model reduction, which preserves the input−output stability of the plant. Model predictive controllers are formulated on that basis to realize model stabilization and account for the input and output constraints. For state estimation, an observer-based MPC realization is proposed and realized by solving the corresponding operator Riccati equation, which is utilized in the construction of Luenberger observer gains. Finally, two numerical examples are provided to demonstrate the feasibility of the proposed MPC design. They show that for the tubular reactor, the proposed MPC is capable of steering the original dynamics to steady states at a faster convergence rate without violating physical constraints and make a good performance in the presence of disturbances. The developed framework can be extended to the MPC design of linear hyperbolic systems with complex reversible reactions (such as $aA + bB \rightleftharpoons rR + sS$) to account for general esterification, saponification, and neutralization reactions.

ASSOCIATED CONTENT

Supporting Information

The Supporting Information is available free of charge at https://pubs.acs.org/doi/10.1021/acs.iecr.0c02500.

Derivations of $\mathcal{A}^*$ and C^* and the link between the discrete Lyapunov equation and the continuous Lyapunov equation under the Cayley−Tustin time-discretization frame (PDF)

AUTHOR INFORMATION

Corresponding Author

Stevan Dubljevic − *Department of Chemical and Materials Engineering, University of Alberta, Edmonton T6G 2V4, Canada;* orcid.org/0000-0002-1889-1599; Phone: +1 780 2481596; Email: Stevan.Dubljevic@ualberta.ca; Fax: +1 780 4922881

Authors

Lu Zhang − *Department of Chemical and Materials Engineering, University of Alberta, Edmonton T6G 2V4, Canada;* orcid.org/0000-0002-4499-9843

Junyao Xie − *Department of Chemical and Materials Engineering, University of Alberta, Edmonton T6G 2V4, Canada;* orcid.org/0000-0002-1949-1909

Charles Robert Koch − *Department of Mechanical Engineering, University of Alberta, Edmonton T6G 2R3, Canada;* orcid.org/0000-0002-6094-5933

Complete contact information is available at: https://pubs.acs.org/10.1021/acs.iecr.0c02500

Notes

The authors declare no competing financial interest.

REFERENCES

(1) Ray, W. H. *Advanced Process Control*; McGraw-Hill: New York, 1981.

(2) Armbruster, D.; Göttlich, S.; Herty, M. A scalar conservation law with discontinuous flux for supply chains with finite buffers. *SIAM J. Appl. Math.* **2011**, *71*, 1070−1087.

(3) Douglas, J. M.; Rippin, D. W. T. Unsteady state process operation. *Chem. Eng. Sci.* **1966**, *21*, 305−315.

(4) Rippin, D. W. T. Recycle Reactor as a Model of Incomplete Mixing. *Ind. Eng. Chem. Fundam.* **1967**, *6*, 488−492.

(5) Douglas, J. M.; Gaitonde, N. Y. Analytical Estimates of Performance of Chemical Oscillators. *Ind. Eng. Chem. Fundam.* **1967**, *6*, 265−276.

(6) Kwon, J.; Nayhouse, M.; Orkoulas, G.; Christofides, P. D. Crystal shape and size control using a plug flow crystallization configuration. *Chem. Eng. Sci.* **2014**, *119*, 30−39.

(7) Aksikas, I.; Winkin, J. J.; Dochain, D. Optimal LQ-feedback regulation of a nonisothermal plug flow reactor model by spectral factorization. *IEEE Trans. Automat. Contr.* **2007**, *52*, 1179−1193.

(8) Aksikas, I.; Winkin, J. J.; Dochain, D. Asymptotic stability of infinite-dimensional semilinear systems: Application to a non-isothermal reactor. *Syst. Contr. Lett.* **2007**, *56*, 122−132.

(9) Liu, L.; Huang, B.; Dubljevic, S. Model predictive control of axial dispersion chemical reactor. *J. Process Control* **2014**, *24*, 1671−1690.

(10) Vasičkaninová, A.; Bakošová, M.; Oravec, J.; Mészáros, A. Model Predictive Control of a Tubular Chemical Reactor. *2019 22nd International Conference on Process Control (PC19)*; IEEE, 2019; pp 228−233.

(11) Rodrigues, D.; Billeter, J.; Bonvin, D. Semi-analytical solutions for tubular chemical reactors. *Chem. Eng. Sci.* **2017**, *172*, 239−249.

(12) Qian, H.; Beard, D. A. Thermodynamics of stoichiometric biochemical networks in living systems far from equilibrium. *Biophys. Chem.* **2005**, *114*, 213−220.

(13) Demirel, Y. Modeling of thermodynamically coupled reaction-transport systems. *Chem. Eng. J.* **2008**, *139*, 106−117.

(14) Constales, D.; Yablonsky, G. S.; D'hooge, D. R.; Thybaut, J. W.; Marin, G. B. *Advanced Data Analysis and Modelling in Chemical Engineering*; Elsevier, 2016.

(15) Denn, M. M. Optimal linear control of distributed systems. *Ind. Eng. Chem. Fundam.* **1968**, *7*, 410−413.

(16) Koppel, L. B.; Shih, Y.-P.; Coughanowr, D. R. Optimal feedback control of a class of distributed-parameter systems with

space-independent controls. *Ind. Eng. Chem. Fundam.* **1968**, *7*, 286−295.
(17) Bošković, D. M.; Krstić, M. Backstepping control of chemical tubular reactors. *Comput. Chem. Eng.* **2002**, *26*, 1077−1085.
(18) Smyshlyaev, A.; Krstic, M. Backstepping observers for a class of parabolic PDEs. *Syst. Contr. Lett.* **2005**, *54*, 613−625.
(19) Aksikas, I.; Winkin, J. J.; Dochain, D. Optimal LQ-feedback control for a class of first-order hyperbolic distributed parameter systems. *ESAIM Control, Optim. Calc. Var.* **2008**, *14*, 897−908.
(20) Mohammadi, L.; Aksikas, I.; Dubljevic, S.; Forbes, J. F. Optimal boundary control of coupled parabolic PDE−ODE systems using infinite-dimensional representation. *J. Process Control* **2015**, *33*, 102−111.
(21) Rippin, D. W. T. Simulation of single-and multiproduct batch chemical plants for optimal design and operation. *Comput. Chem. Eng.* **1983**, *7*, 137−156.
(22) Sundmacher, K.; Qi, Z. Conceptual design aspects of reactive distillation processes for ideal binary mixtures. *Chem. Eng. Process* **2003**, *42*, 191−200.
(23) Georgakis, C. A model-free methodology for the optimization of batch processes: Design of dynamic experiments. *IFAC Proc. Vol.* **2009**, *42*, 536−541.
(24) Richalet, J.; Testud, J.; Rault, A.; Papon, J. Model Predictive Heuristic Control: Applications to Industial Processes. *Automatica* **1978**, *14*, 413−428.
(25) Rawlings, J. B. Tutorial overview of model predictive control. *IEEE Contr. Syst. Mag.* **2000**, *20*, 38−52.
(26) Qin, S. J.; Badgwell, T. A. A survey of industrial model predictive control technology. *Contr. Eng. Pract.* **2003**, *11*, 733−764.
(27) Shang, H.; Forbes, J. F.; Guay, M. Model predictive control for quasilinear hyperbolic distributed parameter systems. *Ind. Eng. Chem. Res.* **2004**, *43*, 2140−2149.
(28) Kumar, A. S.; Ahmad, Z. Model predictive control (MPC) and its current issues in chemical engineering. *Chem. Eng. Commun.* **2012**, *199*, 472−511.
(29) Xie, W.; Bonis, I.; Theodoropoulos, C. Data-driven model reduction-based nonlinear MPC for large-scale distributed parameter systems. *J. Process Control* **2015**, *35*, 50−58.
(30) Marquez, A.; Oviedo, J. J. E.; Odloak, D. Model reduction using proper orthogonal decomposition and predictive control of distributed reactor system. *J. Contr. Sci. Eng.* **2013**, *1025*, 1−19.
(31) Lao, L.; Ellis, M.; Christofides, P. D. Economic model predictive control of transport-reaction processes. *Ind. Eng. Chem. Res.* **2014**, *53*, 7382−7396.
(32) Joy, P.; Rossow, K.; Jung, F.; Moritz, H.-U.; Pauer, W.; Mitsos, A.; Mhamdi, A. Model-based control of continuous emulsion co-polymerization in a lab-scale tubular reactor. *J. Process Control* **2019**, *75*, 59−76.
(33) Zavala, V. M.; Biegler, L. T. Optimization-based strategies for the operation of low-density polyethylene tubular reactors: nonlinear model predictive control. *Comput. Chem. Eng.* **2009**, *33*, 1735−1746.
(34) Dufour, P.; Touré, Y.; Blanc, D.; Laurent, P. On nonlinear distributed parameter model predictive control strategy: on-line calculation time reduction and application to an experimental drying process. *Comput. Chem. Eng.* **2003**, *27*, 1533−1542.
(35) Bonis, I.; Xie, W.; Theodoropoulos, C. A linear model predictive control algorithm for nonlinear large-scale distributed parameter systems. *AIChE J.* **2012**, *58*, 801−811.
(36) Xu, Q.; Dubljevic, S. Linear model predictive control for transport-reaction processes. *AIChE J.* **2017**, *63*, 2644−2659.
(37) Dubljevic, S.; Humaloja, J.-P. Model predictive control for regular linear systems. *Automatica* **2020**, *119*, 109066.
(38) Franklin, G. F.; Powell, J. D.; Workman, M. L., et al. *Digital Control of Dynamic Systems*; Addison-wesley Menlo Park: CA, 1998; Vol. *3*.
(39) Havu, V.; Malinen, J. The Cayley transform as a time discretization scheme. *Numer. Funct. Anal. Optim.* **2007**, *28*, 825−851.
(40) Havu, V.; Malinen, J. Laplace and Cayley transforms-an approximation point of view. *Proceedings of the 44th IEEE Conference on Decision and Control*; IEEE, 2005; pp 5971−5976.
(41) Baaiu, A.; Couenne, F.; Lefevre, L.; Le Gorrec, Y.; Tayakout, M. Structure-preserving infinite dimensional model reduction: Application to adsorption processes. *J. Process Control* **2009**, *19*, 394−404.
(42) Vu, N. M. T.; Lefèvre, L.; Nouailletas, R.; Brémond, S. Symplectic spatial integration schemes for systems of balance equations. *J. Process Control* **2017**, *51*, 1−17.
(43) Moulla, R.; Lefévre, L.; Maschke, B. Pseudo-spectral methods for the spatial symplectic reduction of open systems of conservation laws. *J. Comput. Phys.* **2012**, *231*, 1272−1292.
(44) Curtain, R. F.; Oostveen, J. C. *Bilinear Transformations between Discrete-And Continuous-Time Infinite-Dimensional Linear Systems*; North Carolina State University. Center for Research in Scientific Computation, 1997.
(45) Hahn, D. R.; Fan, L. T.; Hwang, C. L. Optimal startup control of a jacketed tubular reactor. *AIChE J.* **1971**, *17*, 1394−1401.
(46) Badillo-Hernandez, U.; Alvarez, J.; Alvarez-Icaza, L. Efficient modeling of the nonlinear dynamics of tubular heterogeneous reactors. *Comput. Chem. Eng.* **2019**, *123*, 389−406.
(47) Aksikas, I. Analysis and LQ-optimal control of infinite-dimensional semilinear systems: Application to a plug flow reactor. Ph.D. Thesis, UCL, 2005.
(48) Curtain, R. F.; Zwart, H. *An Introduction to Infinite-Dimensional Linear Systems Theory*; Springer, 1995.
(49) Rawlings, J. B.; Mayne, D. Q.; Diehl, M. *Model Predictive Control: Theory, Computation, and Design*; Nob Hill Publishing Madison: WI, 2017; Vol. *2*.
(50) Muske, K. R.; Rawlings, J. B. Model predictive control with linear models. *AIChE J.* **1993**, *39*, 262−287.
(51) Tucsnak, M.; Weiss, G. *Observation and Control for Operator Semigroups*; Springer Science & Business Media, 2009.
(52) Dochain, D. State and parameter estimation in chemical and biochemical processes: a tutorial. *J. Process Contr.* **2003**, *13*, 801−818.
(53) Xie, J.; Xu, Q.; Ni, D.; Dubljevic, S. Observer and filter design for linear transport-reaction systems. *Eur. J. Contr.* **2019**, *49*, 26−43.
(54) Xu, X.; Dubljevic, S. Output regulation problem for a class of regular hyperbolic systems. *Int. J. Contr.* **2016**, *89*, 113−127.
(55) Xie, J.; Koch, C. R.; Dubljevic, S. Discrete Output Regulator Design for Linear Distributed Parameter Systems. *Int. J. Contr.* **2020**, 1−17.
(56) Muske, K. R. Linear model predictive control of chemical processes. Ph.D. Thesis, University of Texas at Austin, 1995.

https://dx.doi.org/10.1021/acs.iecr.0c02500
Ind. Eng. Chem. Res. 2020, 59, 18921−18936